

Impact of axonal delay on structure development in a multi-layered network

Catherine E. Davey^a, David B. Grayden^a, and Anthony N. Burkitt^a

^a*Department of Biomedical Engineering, The University of Melbourne, VIC 3010, Australia*

November 30, 2020

Keywords: neural network, rate-based neural plasticity, axonal propagation delay, spatial opponent cells

Abstract

The mechanisms underlying how random activity in the visual pathway could give rise through neural plasticity to many of the features observed experimentally in the early stages of visual processing was provided by Linker in a seminal, three-paper series. Owing to the complexity of multi-layer models, by Linker in a licit assumption in Linker's and subsequent papers has been that propagation delay is homogeneous and, consequently, plays little functional role in neural behaviour. In this paper, we relax this assumption to examine the impact of distance-dependent axonal propagation delay on neural learning. We show that propagation delay induces low-pass filtering by dispersing the arrival times of spikes from presynaptic neurons, providing a natural correlation cancellation mechanism for distal connections. The cut-off frequency decreases as the radial propagation delay within a layer increases relative to propagation delay between the layers, introducing an upper limit on temporal resolution. Given that the post-synaptic potential (PSP) also acts as a low-pass filter, we show that the effective time constant of each should enable the processing of similar scales of temporal information. This result has implications for the visual system, in which receptive field size and, thus, radial propagation delay, increases with eccentricity. Furthermore, the network response is frequency dependent since higher frequencies require increased input amplitude to compensate for attenuation. This concurs with frequency-dependent contrast sensitivity in the visual system, which changes with eccentricity and receptive field size. We further show that the proportion of inhibition relative to excitation is larger where radial propagation delay is long relative to inter-laminar propagation delay. We show that the addition of propagation delay reduces the range in the size of the spatial opponent cell's on-center size, providing stability to variations in homeostatic parameters across a feature map.

1 Introduction

Synaptic plasticity describes the process by which changes to synaptic weights between neurons occur in response to their activities. The development of mathematical models of plasticity has been instrumental in furthering our understanding of the formation of receptive fields of simple cells in primary visual cortex (V1). Linker (1986a,b,c) showed how cells sensitive to simple features, such as orientation, can develop across several neural layers in the absence of structured input, demonstrating how spatial structure in cortical connections is sufficient to drive a self-organization learning process. There has subsequently been much progress in our understanding of the plasticity mechanisms that drive learning of simple features. An important component of this work has been the development of a rigorous mathematical framework from which to interrogate properties of plasticity and neural network development (MacKay and Miller, 1990; Wimbauer et al., 1998).

Development of a rigorous mathematical framework to express Hebbian learning on a network scale has been crucial in advancing our understanding of the formation of simple cells and feature maps in the early stages of learning (Miller, 1990). Owing to the complexity of models resulting from multiple layers of structured input, there has been limited work that has

addressed the impact of axonal delay on the development of simple features, with none incorporating the impact of delay both within and between layers. Wimbauer et al. (1997) showed the development of direction selective cells in response to a combination of lagged and non-lagged input via empirical simulation, although the impact of propagation delay was assumed to be negligible. Leibold et al. (2001) provided a mathematical description of the evolution of a temporal feature map, highlighting the importance of temporal parameters in the neuron model and learning function but not incorporating spatially dependent delay. Leibold and van Hemmen (2001) showed the evolution of temporal feature maps for sound localization, employing a one-dimensional spatial structure.

An implicit assumption of most of these papers has been that spike propagation is instantaneous or, equivalently, that the interlaminar distance is sufficiently greater than radial distances between neurons to permit the assumption that propagation time is approximately equal for all spikes received by a neuron. This assumption enables correlation between neural outputs to be evaluated without spatially induced delay. However, experimental work demonstrates that propagation delay is important. For example, Saam and Eckhorn (2000) showed that spike conduction velocity impacts the spatial range of synchronization and the subsequent receptive field sizes of cells. Kremkow et al. (2016) noted the importance of controlling the delay of excitation and inhibition in broadening the range of statistics that sensory cortical neurons can process. The importance of propagation delay has also been highlighted in the context of synaptic plasticity. Eguchi et al. (2014) discuss the role of propagation delay in developing clusters of cells via spike-timing-dependent plasticity (STDP), while Asl et al. (2017) explore the impact of propagation delay on emerging network structure with STDP as a result of spike arrival order being disrupted. Furthermore, the advantageous arrangement of conduction delay via propagation length or axon diameter to cause coincident spike arrival at postsynaptic neurons has been long noted, such as in giant squid axons (Pumphrey and Young, 1938) and the barn owl (Carr and Konishi, 1988).

While the importance of spike timing for synaptic plasticity has been well motivated, the modelling of propagation delay to understand its impact on the evolution of receptive field structure is still in its infancy. In this paper, we examine the impact of three-dimensional propagation delay on the emergence of V1 simple cells using Linsker’s three layer network model. We analytically derive the impact of spike propagation delay on the neural activity of postsynaptic cells and determine an expression for covariance between neurons that incorporates radial propagation delay determined from synaptic connectivity radius, spike propagation velocity, cell density, inter-laminar propagation delay, and an exponentially decaying post-synaptic potential (PSP). We show that propagation delay effectively acts as a low-pass filter, filtering out high frequencies of the inputs by spreading out the arrival time of presynaptic signals to the cell. We further show that the ratio of propagation delay between neural layers to the radial delay within a layer is the most important factor in determining the extent of attenuation of the high frequencies. In deriving the impact of propagation delay on covariance between presynaptic inputs and, hence, on neural plasticity, we show that, while delay spreads out the arrival times of spikes and, hence, decimates covariance between presynaptic neurons, the PSP is crucial in restoring covariance, as it temporally spreads the impact of a single spike. Given that a PSP also acts as a low-pass filter, we propose that the cut-off frequencies for each will be compatible. This may partly explain the different synaptic time constants found in peripheral and foveal ganglion cells, which can differ by up to a factor of 2 (Zhao et al., 2016). It may also explain why contrast sensitivity is frequency dependent in the periphery, and why the cut-off frequency increases with eccentricity (Virsu et al., 1982). It also provides an insight into why spatial and temporal frequency processing in the visual cortex are not independent (Zhao et al., 2016; Venkataraman et al., 2017). To simplify application of propagation delay in neural models, we derive a mathematically simple approximation and demonstrate its accuracy across a range of parameter configurations.

Finally, we show that the size of the on-centre compared to the off-surround of a resultant V1 cell is a function of the fixed point mean synaptic weight, which can be determined from the homeostatic constants and covariance between presynaptic inputs. For smaller fixed point mean weights, there will be relatively fewer excitatory inputs and more inhibitory inputs. This is in agreement with the synaptic arrangement of ganglion cells, which have significantly more inhibitory inputs in the periphery, where the cells are more spread across the laminar and the impact of radial propagation delay will be greatest (Sinha et al., 2017). We show that propagation delay limits the range of receptive field sizes that can emerge from learning.

2 Methods

2.1 Specification of the network

We employ the topographic network proposed by Linsker (1986a), which comprises three layers, *A*, *B*, and *C*, with feedforward connections from layer *A* to *B* and from layer *B* to *C*, as illustrated in Fig. 1. We remain faithful to Linsker’s notion of a simple

network with a minimal set of assumptions to identify the fundamental principles driving the emergence of cortical structure (Linsker, 1986a). The layers are positioned as planes parallel to one another with neurons equispaced in a square grid within each lamina. Connections between layers are learned sequentially, such that synapses from A to B are learned to maturity before connections from B to C are learned. To aid interpretation of distance metrics, we measure distances across a lamina in terms of number of grid spaces. Connections between layers have a spatial distribution such that nearby neurons in the presynaptic layer are more densely connected to a postsynaptic neuron in the overlying layer.

As the radial distance from the postsynaptic neuron increases, connection density decreases as a Gaussian function of the distance. Define the two-dimensional radial distance of presynaptic neuron, m , from postsynaptic neuron, i , by a vector, (x_{mi}, y_{mi}) . The density of connections from layer A to the subsequent layer B is parameterized by the radius, $(\sigma^{AB})^2$, which is the distance-dependent variance of the Gaussian distributed connection probability, measured in grid spaces, μ^A , to ensure scaling with cell density in the lamina. Consequently, the probability of presynaptic neuron, m , in layer A generating a synaptic connection to postsynaptic neuron, i , in layer B is given by

$$p_N \left((x_{mi}, y_{mi}) ; \frac{1}{2}(\sigma^{AB})^2 \right) = \frac{1}{\pi(\sigma^{AB})^2} \exp \left(-\frac{x_{mi}^2 + y_{mi}^2}{(\sigma^{AB})^2} \right). \quad (1)$$

Note that this definition differs from the standard definition by a factor of $\sqrt{2}$; it has been specifically chosen for later convenience.

Similarly, the distribution of presynaptic connections from layer B to layer C is Gaussian, parameterized by $(\sigma^{BC})^2$. Without loss of generality, we can assume that a layer C cell is in the center of the lamina, and write the probability of a B cell making a connection to the layer C cell using polar coordinates,

$$p_N \left((r_{ip}, \theta_{ip}) ; (\sigma^{BC})^2 \right) = \frac{1}{\pi(\sigma^{BC})^2} \exp \left(-\frac{r_{ip}^2}{(\sigma^{BC})^2} \right), \quad (2)$$

where r_{ip} is the radial distance from the center of the lamina to i and θ_{ip} is the angle to i within the two-dimensional lamina.

The expected number of shared presynaptic inputs between two postsynaptic neurons in layer B can easily be shown to be (see Appendix A for full derivation)

$$\mathbb{E} \left[N^{BB}(d) \right] = \frac{(N^{AB})^2}{2\pi(\sigma^{AB})^2} \exp \left(-\frac{(d_{ij}^B)^2}{2(\sigma^{AB})^2} \right), \quad (3)$$

where d_{ij}^B depicts the distance between neurons i and j such that $d_{ij}^B = \sqrt{x_{mi}^2 + y_{mi}^2}$, measured in grid spaces, μ^A .

An action potential takes time to propagate along an axon. It is generally accepted that, for myelinated axons, transmission time is linearly proportional to the distance propagated (Asl et al., 2017). We introduce a model of transmission delay in which delay is a deterministic and linear function of the three-dimensional distance between the presynaptic and postsynaptic neurons, including both inter- and intra-lamina distances, and is inversely proportional to the speed of propagation. Given that axonal propagation delay typically dominates dendritic propagation delay, we make an assumption that dendritic delay is approximately equal for all cells and, therefore, that distant-dependent delay can be calculated from axonal propagation delay.

Let the radial distance of a presynaptic neuron, m , in layer A to a postsynaptic neuron, i , in layer B be given by the magnitude of the (x_{mi}, y_{mi}) vector and designated d_{mi}^B . For Gaussian x_{mi} and y_{mi} , this distance is characterized by a Rayleigh distribution, so that if $(\sigma^{AB})^2$ denotes the connection radius of the Gaussian connections, then the radial distance between neurons in the presynaptic layer A connecting to postsynaptic neuron i has distribution $d_{mi}^B \sim \mathcal{Rayl} \left(0, \frac{(\sigma^{AB})^2}{2} \right)$. Furthermore, the probability of neuron m making a synaptic connection to neuron i from a radial distance d_{mi}^B is

$$p_{\text{Rayl}} \left(d_{mi}^B ; \frac{(\sigma^{AB})^2}{2} \right) \sim \frac{2d_{mi}^B}{(\sigma^{AB})^2} \exp \left(-\frac{(d_{mi}^B)^2}{(\sigma^{AB})^2} \right). \quad (4)$$

Denoting transmission delay between neuron m in layer A and neuron i in layer B by Δ_{mi}^{AB} and assuming an interlaminar distance of d^{AB} , propagation delay from m to i can be expressed as

$$\Delta_{mi}^{AB} = \frac{((d^{AB})^2 + (d_{mi}^B)^2)^{1/2} \mu^A}{v}, \quad (5)$$

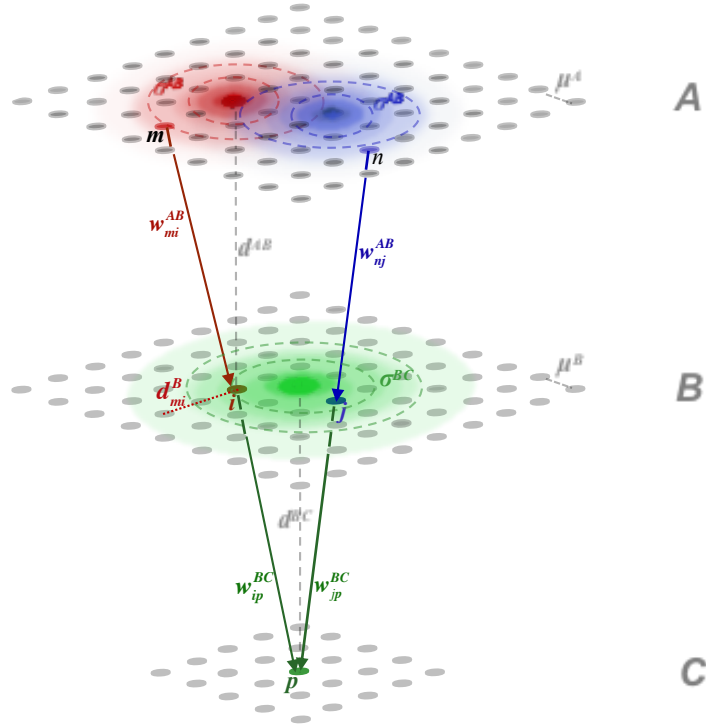


Figure 1: Diagram of a three layer feed-forward network, with neurons m and n in layer A connecting to neurons i and j , respectively, in layer B ; both neurons i and j in layer B connect to neuron p in layer C . Each postsynaptic neuron has been color coded to aid interpretation, such that neuron i has been colored red, neuron j is blue, and neuron p is green. The synaptic connection density of a postsynaptic neuron determines the probability of a neuron in the presynaptic layer connecting to it and is depicted by the density of that neuron's color in the presynaptic layer. Connection density is modelled as Gaussian, with parameters constant across a layer, so that σ^{AB} denotes the radius, or standard deviation, of connections between layers A and B , while σ^{BC} denotes the radius of connections between layers B and C . The first and second standard deviations of the Gaussian connection probability for a postsynaptic neuron are represented by colored, dashed concentric circles in the presynaptic layer of the neuron. Interlaminar distance between layers A and B is denoted d^{AB} , while distance between layers B and C is denoted by d^{BC} . The radial distance between two neurons within a lamina, for example between neuron m from layer A and i from layer B , is denoted d_{mi}^B . Distance metrics are given in grid spaces, μ^A and μ^B , respectively, which are in themselves measured in μm , to separate out the effect of cell density. The strength of a synaptic connection between two neurons, for example between neurons j and i , is given by w_{ji}^{BC} . Not shown in the diagram are N^{AB} and N^{BC} , which represent the expected number of synaptic connections to each postsynaptic neuron in layers B and C , respectively.

where v is the spike propagation velocity and μ^A is the distance between neurons in the lamina in μm . The distance metrics, including d^{AB} and d_{mi}^B , are measured in grid spaces, μ^A , to separate out the effect of cell density from other distance measures such as connectivity radii and inter-laminar distance.

2.2 Neuron model

To simplify the analysis of a multi-layer neural network with propagation delay, we employ a Poisson neuron model. Poisson models are simple in that activity is a linear sum of inputs weighted by synaptic strength and that spike thresholds and reset are not modeled. Although it is a simple model, Kempter et al. (1999) noted that large networks of integrate-and-fire neurons exhibit Poisson firing characteristics. The network is driven by spontaneous activity from layer A , modelled as a homogeneous Poisson process with rate, λ^A .

2.2.1 Linsker's neuron model

Using a Poisson model, the firing rate of the postsynaptic neurons can be described by

$$f_i^B(t) = R_a^B + \sum_m w_{mi}^{AB}(t) f_m^A(t), \quad (6a)$$

$$f_p^C(t) = R_a^C + \sum_j w_{jp}^{BC}(t) f_j^B(t), \quad (6b)$$

where a neuron, m , in layer A provides feedforward input to a neuron, i , in layer B , and a neuron, j , in layer B provides feedforward input to a neuron, p , in layer C , under an assumption of instantaneous propagation, R_a^B denotes background activity, and w_{mi}^{AB} depicts synaptic strength between neurons m and i . Note that this differs from Linsker (1986a) by a dimensionless scale factor of R_b^{AB} applied to the sum that we have absorbed into the weights. The calculation of the variance of neural activity in B is given in Appendix B.

It is useful to introduce frequency domain definitions of the temporal signals. Spectral signals will, in general, be denoted by the upper-case counterpart to the lower-case symbol designating the temporal variable. For example, F_m denotes the frequency domain variable of neuronal rate, f_m . From the definition of the Fourier transform and under the assumption of stationarity (i.e. slow weight evolution), the unfiltered rate can be expressed as a function of spectral variates using the inverse Fourier transform,

$$f_m^B(t) = \frac{1}{T} \sum_k F_m^B(k) \exp(2\pi i t k'), \quad F_m^B(k) = \sum_t f_m^B(t) \exp(-2\pi i t k'), \quad (7)$$

where \sum_k and \sum_t are shorthand notations for $\sum_{k=0}^{T-1}$ and $\sum_{t=0}^{T-1}$ and $k' = \frac{k}{T}$, respectively, to aid readability.

2.2.2 Network incorporating propagation delay and a general postsynaptic response

To model the temporal dynamics of a synapse's membrane potential, we introduce the post-synaptic potential (PSP), ε , which, for rate-based neuronal activity, this can be interpreted as spikes having a probability distribution over time. For example, the spike rates from Eq. (6) are generalised to incorporate an arbitrary PSP by

$$(f_i^B \star \varepsilon)(t) = R_a^B + \sum_m w_{mi}^{AB} (f_m^A \star \varepsilon)(t), \quad (8a)$$

$$(f_p^C \star \varepsilon)(t) = R_a^C + \sum_i w_{ip}^{AC} (f_i^B \star \varepsilon)(t), \quad (8b)$$

where \star is the convolution operator and $(f_i^B \star \varepsilon)$ denotes firing rate that has been filtered by the PSP. The PSP is typically assumed to integrate to 1; i.e., $\int_0^\infty \varepsilon(s) ds = 1$.

Since convolution in the temporal domain is multiplication in the frequency domain, neural output that has been filtered by a PSP kernel, as defined in Eq. (8), can be expressed using frequency variables by employing the Fourier transform from Eq. (7) to give

$$(f_i^B \star \varepsilon)(t) = \frac{1}{T} \sum_k F_i^B(k) E(k) \exp(2\pi i t k'), \quad (9)$$

where $E(k)$ denotes the PSP in the frequency domain at frequency k . Note that since the temporal signals are real, the imaginary frequency components of the PSP filter are conjugate symmetric around 0.

Relaxing the assumption of homogeneous propagation and denoting the rate for neuron i that is a function of both the synapse response kernel and propagation delay by $(f_i^{B(\Delta)} \star \varepsilon)$, the expressions for neuronal spiking rates in layers B and C as a function of input become

$$(f_i^{B(\Delta)} \star \varepsilon)(t) = R_a^B + \sum_m w_{mi}^{AB} f_m^A(t - \Delta_{mi}^{AB}) \star \varepsilon(t), \quad (10a)$$

$$(f_p^{C(\Delta)} \star \varepsilon)(t) = R_a^C + \sum_i w_{ip}^{BC} (f_i^{B(\Delta)} \star \varepsilon)(t - \Delta_{ip}^{BC}) \star \varepsilon(t). \quad (10b)$$

For simplicity, we suppose that neurons in all layers have the same PSP. However, it is straightforward to incorporate layer-specific PSP functions.

By the linearity of the Fourier transform, Eq. (7), rate can be written as a sum of the input spectral variates. For unitary weights from layer $A \rightarrow B$ and letting $k' = \frac{k}{T}$ for readability, the neuronal activity model that incorporates propagation delay in Eq. (10) can be written as

$$(f_i^{B(\Delta)} \star \varepsilon) = \frac{1}{T} \sum_k \exp(2\pi i t k') \sum_m F_m^A(k) E(k) \exp(-2\pi i \Delta_{mi} k') \quad (11)$$

2.3 Neural learning in Linsker's network

2.3.1 Covariance of neural activity

Linsker (1986a) showed that spatial structure in synaptic connections between layers creates temporal covariance in neural activity between cells in layer B and onward. A Gaussian synaptic connection density ensures that layer B neurons situated nearer to each other in the lamina have more layer A connections in common and, consequently, the neural activities of these neurons are more correlated. Layer B neurons are the presynaptic inputs to layer C neurons, also connected with a Gaussian density, parameterized by a unique connectivity radius, $(\sigma^{BC})^2$. The layer B neurons located radially closer to the postsynaptic neuron in layer C will have more nearby neighbors that are also connected to the postsynaptic layer C neuron and, being located near each other, will have more layer A connections in common and so will be more temporally correlated. Thus, a spatial structure in temporal covariance is created. Linsker (1986a) demonstrated that the resulting structure in temporal covariance can generate the emergence of receptive field structure in deeper layers via Hebbian learning, showing the creation of spatial opponent cells in layer C and orientation selective cells in layers deeper in the hierarchy.

Since learning is driven by the covariance of presynaptic neural activity (Kempster et al., 1999), we derive an expression for covariance between layer B neurons, as given by Linsker (1986a). Initially, we consider learning in an ideal network, such as Linsker (1986a) employed, in which there is uniform propagation delay across all neurons and an implied delta function for the postsynaptic response.

Using the expression for the expected number of shared connections between layer B neurons in Eq. (3), the covariance is given by (see Appendix C)

$$\text{cov}(f_i^B, f_j^B) = \frac{(N^{AB})^2 (\lambda^A)^2}{2\pi(\sigma^{AB})^2} \exp\left(-\frac{d^2}{2(\sigma^{AB})^2}\right). \quad (12)$$

This expression for covariance between layer B neurons is pivotal in determining the final synaptic structure for a stable network (Linsker, 1986a).

Since instantaneous covariance is equivalent to the cross-correlation of zero-meaned variates at lag 0 (see Appendix D for details), we can use Eq. (7) to express covariance between two layer B neurons as

$$\begin{aligned} \text{cov}(f_i^B, f_j^B) &= \frac{1}{T^2} \sum_k (F_i^B(k))^* F_j^B(k) \exp\left(2\pi i 0 \frac{k}{T}\right) \\ &= \frac{1}{T^2} \sum_k (F_i^B(k))^* F_j^B(k). \end{aligned} \quad (13)$$

In the following, when considering neural learning of synapses between layers B and C , it is assumed that synapses between layers A and B have already evolved to maturity such that all synapses are excitatory with unity weight (see Linsker (1986a) for conditions required for this to occur). Therefore, we will consider the plasticity of B to C connections in this work.

2.3.2 Learning equation

Synaptic plasticity occurs adiabatically when compared with neuronal dynamics as it is the result of many incremental changes in synapse strength. Furthermore, each neuron within a layer has identical spatial connectivity and firing rate statistics.

Consequently, the system can be considered ergodic. This is significant because it enables statistics, such as covariance in neuronal firing rate, to be evaluated either by taking an ensemble average or a temporal average over a trial or epoch.

Linsker (1986a) assumed that a synapse between two neurons was potentiated if the product of the pre- and post-synaptic neuronal activity was above average, indicating that their activity positively covaried, and vice-versa. We can take advantage of the slow change in synaptic weights and the ergodicity of the system by taking an ensemble average of weights across the lamina. The learning equations for synaptic weights can then be expressed as first-order linear differential equations (Linsker, 1986a),

$$\dot{w}_{mi}^{AB} \triangleq \eta \langle (\Delta w_{mi}^{AB}) \rangle = \eta \left(k_1^{AB} + \frac{1}{N^{AB}} \sum w_{ni}^{AB} (Q(f_n^A, f_m^A) + k_2^{AB}) \right), \quad w_{\min}^{AB} \leq w_{mi}^{AB} \leq w_{\max}^{AB}, \quad (14a)$$

$$\dot{w}_{ip}^{BC} \triangleq \eta \langle (\Delta w_{ip}^{BC}) \rangle = \eta \left(k_1^{BC} + \frac{1}{N^{BC}} \sum w_{jp}^{BC} (Q(f_j^B, f_i^B) + k_2^{BC}) \right), \quad w_{\min}^{BC} \leq w_{ip}^{BC} \leq w_{\max}^{BC}, \quad (14b)$$

where $\eta \ll 1$ is the learning rate, chosen to be sufficiently small such that the weights are quasi-constant on the timescale of neuronal dynamics, w_{mi}^{AB} depicts the weight of the synapse connecting presynaptic neuron n in layer A to postsynaptic neuron i in layer B , and, similarly, w_{jp}^{BC} depicts the weight of the synapse connecting presynaptic neuron j in layer B to postsynaptic neuron p in layer C . The parameters k_1^{AB} , k_2^{AB} , and k_1^{BC} , k_2^{BC} are learning constants that are homogeneous across all synapses connecting two neural populations. $Q(f_n^A, f_m^A)$ and $Q(f_j^B, f_i^B)$ denote the expected covariance in neural activity between neurons n and m in layer A and neurons i and j in layer B , respectively. The definition for each follows the same structure that, for layer B covariance as an example, is $Q(f_j^B, f_i^B) = f_0^{-2} \langle f_i^B - \bar{f}^B \rangle \langle f_j^B - \bar{f}^B \rangle$, where $\langle \rangle$ denotes an ensemble average, f_i^B is the rate of activity of neuron i in layer B , \bar{f}^B is the temporal average of layer B spiking rates in an ergodic system, and f_0^2 is a scaling factor to normalize the covariance matrix, Q . From the expected value of covariance in Eq. (12), it can be seen that to normalize the covariance requires that

$$\begin{aligned} Q(f_j^B, f_i^B) &= f_0^{-2} \text{cov}(f_i^B, f_j^B) \\ &= \exp\left(-\frac{d^2}{2(\sigma^{AB})^2}\right) \in [0, 1], \end{aligned} \quad (15)$$

such that

$$f_0^2 = \frac{2\pi(\sigma^{AB})^2}{(N^{AB})^2 (\lambda^A)^2}. \quad (16)$$

Inspection of the weight Eqs. (14a) and (14b) shows that k_1 and k_2 do not depend on input and, therefore, do not drive learning, but rather regulate overall activity and determine homeostasis. Without the dependence of the learning equation on input covariance, all weights would evolve to either the upper or lower bound because no presynaptic neuron would be more competitive than another and thus all neurons would change equally.

The weight bounds, $w_{\min} \leq w \leq w_{\max}$, are determined by the proportion of excitatory to inhibitory neurons (Linsker, 1986a). Linsker (1986a) showed that, for a linear network such as this, having a fraction, w_{\max} , of excitatory synapses with limits of 0 and 1, and a fraction, $w_{\min} = 1 - w_{\max}$, of inhibitory synapses with limits of -1 and 0, is equivalent to all synapses having limits of w_{\min} and w_{\max} .

In this work, the term ‘receptive field’ refers to an inter-layer receptive field; i.e., rather than being defined by stimulus space, it is defined by a cortical neuron’s input synaptic weight structure. The receptive field learned by a neuron is described by the set of synaptic weights from its presynaptic neurons after the system has converged to equilibrium. For neuron i in layer B , the set of presynaptic neurons can be described by $\{m \mid m \text{ has a synaptic connection to } i\}$. Denote by $(w_{mi}^{AB})_*$ the fixed point for the synapse weight from neuron m in layer A to neuron i in layer B . The fixed point is assumed to be reached once all synapse weights, or all but one, are no longer changing (Linsker, 1986a). The set of fixed point weights describe the receptive field learned by neuron i . If a synapse has a weight of 0 then it is not considered to be part of the receptive field.

As per Linsker (1986a), the parameters for the layer A to B connection are chosen such that the weights are unstable and all, or all but one, reach the upper bound, w_{\max}^{AB} . In this way, correlations in the neural activity of layer B cells emerge from spatial structure in the presynaptic input from layer A , rather than structure in the connection weights.

3 Results

We derive an analytical expression for neural activity of layer B neurons in the presence of propagation delay. To facilitate the use of this expression in analytical neural networks, we determine a simplified form for the impact of propagation delay. An expression for covariance between layer B neurons is calculated for the case in which an arbitrary PSP is included in the neuron model, Eq. (8), and then for the case in which a PSP and three-dimensional propagation delay is incorporated into the neuron model, Eq. (10). Finally, since we assume that the plasticity mechanism is initiated near the site of a layer C cell body, covariance is calculated for the neural activity of two presynaptic layer B cells at the time this activity is received by the postsynaptic neuron in layer C .

Using the expression for covariance when employing a generalized neuron model that incorporates both propagation delay and arbitrary PSP, a learning equation for synaptic weights is specified. We calculate the expected size of a layer C neuron's receptive field when Linsker's (1986a) neuron model is employed, Eq. (6); i.e., when there is an implicit delta function model of a PSP and inter-lamina delay is implicitly assumed to dominate propagation delay sufficiently such that radial propagation delay is negligible.

Using the expressions derived for covariance between layer B neurons when activity is filtered by an arbitrary PSP, we calculate receptive field size for a layer C neuron. Finally, we analytically determine the receptive field size of a layer C cell in the presence of three-dimensional propagation delay.

3.1 Neural firing rate with propagation delay

Our first result is to analytically derive the output spiking rate of neurons in layer B in the presence of propagation delay. It is known that neurons have an upper bound on the temporal resolution of the neural code carried by the input spikes. The aim of this section is to explore the impact of propagation delay on this upper bound.

For a layer B neuron that receives input spikes delayed according to the spatial layout of its presynaptic neurons and convolved with a PSP kernel (Eq. (11)), the output spiking rate can be expressed via frequency variables as

$$\begin{aligned}
 (f_i^{B(\Delta)} \star \varepsilon) &= \frac{1}{T} \sum_k \exp(2\pi i t k') \sum_m F_m^A(k) E(k) \exp(-2\pi i \Delta_{mi} k') \\
 &= \frac{1}{T} \sum_k \exp(2\pi i t k') E \left[\exp(-2\pi i \Delta_{mi} k') \right] E(k) \sum_m F_m^A(k) \\
 &= \frac{1}{T} \sum_k \exp(2\pi i t k') E \left[\exp(-2\pi i \Delta_{mi} k') \right] E(k) F_i^B(k).
 \end{aligned} \tag{17}$$

Note that all layer A spectral variates are multiplied by the same PSP filter and thus it can come out of the inner sum, leaving a sum of layer A input spectral variates, which gives the same layer B spectral variate as for the no PSP and no delay case. Therefore, it remains to determine the impact of the expected value of delay in the frequency domain to understand its impact on the output rate of a layer B neuron.

Derivation of the expected value of delay in the frequency domain is given in Appendix E. The derivation integrates the Fourier transform of propagation delay, $\exp(-2\pi i \Delta_{mi} k')$, between each presynaptic neuron m and the given postsynaptic neuron i over the presynaptic layer, weighted by the probability of the presynaptic neuron having a connection to the postsynaptic neuron, Eq. (4). Note that delay is determined from the three-dimensional distance between the pre- and post-synaptic neurons, comprised of the radial distance, d_{mi}^B , the interlaminar distance, d^{AB} , and the speed of propagation, v , Eq. (5) (see Fig. 1 for schematic). Given that neurons that are the same distance from the postsynaptic neuron will have the same propagation delay and the same probability of connection, the integration is done in concentric rings of increasing distance from the postsynaptic neuron. Since the integral is over a complex domain, it is solved using contour integration,

$$\begin{aligned}
D^{AB}(k) &= \mathbb{E} \left[\exp(-2\pi i \Delta k') \right] \\
&= \exp \left(-2\pi i k' \frac{d^{AB} \mu}{v} \right) - \pi^{3/2} k' \frac{\sigma^{AB} \mu}{v} \exp \left(\frac{(d^{AB})^2}{(\sigma^{AB})^2} \right) \exp \left(- \left(\pi k' \frac{\sigma^{AB} \mu}{v} \right)^2 \right) \\
&\quad \left(\text{ierfc} \left(\frac{d^{AB}}{\sigma^{AB}} \right) + \text{erf} \left(\frac{d^{AB}}{\sigma^{AB}} + i \pi k' \frac{\sigma^{AB} \mu}{v} \right) - \text{erf} \left(\frac{d^{AB}}{\sigma^{AB}} \right) \right). \tag{18}
\end{aligned}$$

The expression for the mean value of delay in the frequency domain is essentially a function of two parameters,

$$\tau_l = \frac{d^{AB} \mu}{v} ([\tau_l] = s), \quad \tau_r = \frac{\sigma^{AB} \mu}{v} ([\tau_r] = s), \tag{19}$$

where τ_l depicts the propagation time between layers and τ_r represents the radial propagation time within the lamina. Consequently, mean delay in frequency can be written

$$D^{AB}(k) = \exp(-2\pi i k' \tau_l) - \pi^{3/2} k' \tau_r \exp \left(\left(\frac{\tau_l}{\tau_r} \right)^2 \right) \exp \left(- (\pi k' \tau_r)^2 \right) \left(\text{ierfc} \left(\frac{\tau_l}{\tau_r} \right) + \text{erf} \left(\frac{\tau_l}{\tau_r} + i \pi k' \tau_r \right) - \text{erf} \left(\frac{\tau_l}{\tau_r} \right) \right). \tag{20}$$

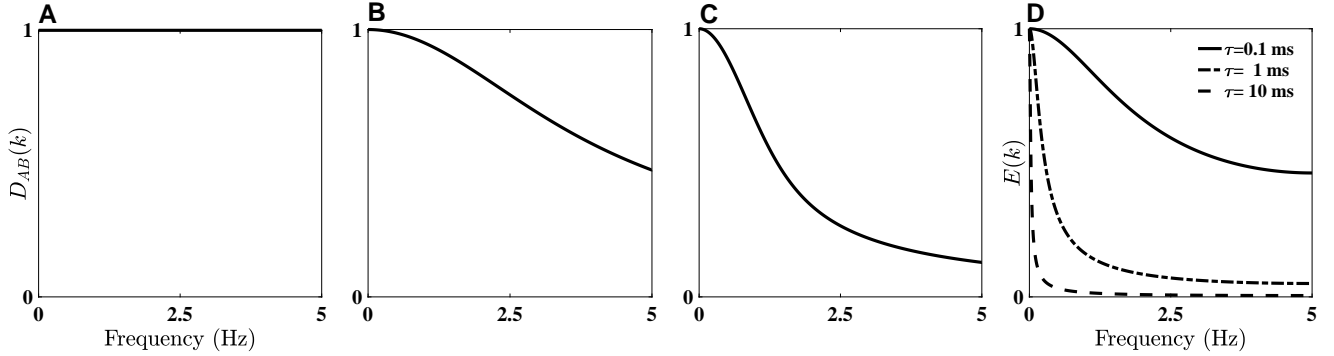


Figure 2: **(A-C)** Magnitude of the expected value of delay Eq. (20), in the frequency domain for different radial propagation delays, τ_r . The x-axis shows frequencies, k' , up to the Nyquist frequency, from 0 to 5 kHz. The y-axis is $D^{AB}(k) \in [0, 1]$. The inter-layer propagation delay was $\tau_l = 500 \mu\text{s}$, derived from velocity, $v = 2$ m/s, and neural density, $\mu = 10 \mu\text{m}$. The radial propagation delay was **(A)** $\tau_r = 50 \mu\text{s}$, **(B)** $\tau_r = 250 \mu\text{s}$, and **(C)** $\tau_r = 500 \mu\text{s}$. **(D)** The magnitude of an example PSP in the frequency domain, normalized between 0 and 1, to enable comparison with frequencies retained in rate-based neural activity after incorporating the impact of propagation delay. In this example, the PSP is modelled with a single parameter, the decay time, τ , such that $\varepsilon \propto \exp(-\frac{t}{\tau})$, so that in the frequency domain $E \propto \frac{\tau}{1+ik'\tau}$, and normalized to 1.

Fig. 2 shows the mean delay as a function of different radial propagation velocities, which is determined by the connection radius, the neuron density, and spike propagation velocity, as detailed in Eq. (19). For comparatively small radial propagation delays relative to inter-layer propagation delay (Fig. 2A), the delay of all spikes from the presynaptic layer to a postsynaptic neuron is approximately equal and the impact of delay is negligible. As the radial propagation delay increases relative to the inter-layer propagation delay, the propagation time from presynaptic neurons to a postsynaptic neuron can no longer be assumed approximately equal and the spread in arrival times to the postsynaptic neuron effectively smooths the input to layer B postsynaptic neurons (Fig. 2B,C). Example frequency profiles for the PSP are shown in Fig. 2D, in which the PSP is modelled as a single exponential function with the decay parameter chosen to reflect the effective membrane time constant, which is shorter than the membrane time constant due to the neuron becoming more leaky as more synaptic channels open (Burkitt et al., 2003). For PSPs with long decay times, its Fourier transform contains only low frequencies and, for inter-lamina distances that dominate radial distances, the propagation delay between layers dominates the radial propagation delay sufficiently such that the mean delay in frequency, $D^{AB}(k) \in [0, 1]$, attenuates only the very highest frequencies. Consequently, propagation delay does not destroy frequencies that are present in the neuronal signal.

The most important factor in determining the impact of propagation delay on neural firing is the ratio of inter-lamina delay to the radial propagation time. Application of the expected value of delay in the frequency domain, Eq. (20), to the derivation of

neural response in the presence of distance-dependent delay gives

$$(f_i^{B(\Delta)} \star \varepsilon) = \frac{1}{T} \sum_k \exp(2\pi i t k') D^{AB}(k) E(k) F_i^B(k). \quad (21)$$

Fig. 3 shows the frequency response for neural spiking rate in layer B , derived in Eq. (21), in response to white noise input from layer A and assuming a PSP modelled as a decaying exponential. The figure shows the mitigating impact of increasing propagation velocity on retaining power across all frequencies, as expected. Also intuitive is the observation that increasing the distance between layers relative to the radial connectivity distance (i.e., increasing the ratio of τ_l to τ_r) reduces the attenuation of high frequencies, though this has a smaller impact than spike propagation velocity. In Fig. 3A and B, propagation delay dominates the frequency response of the layer B neurons, while for Fig. 3C and D, the postsynaptic potential dominates the frequency response. That is, whichever filters out more of the incoming signal – propagation delay or the postsynaptic potential – dominates the frequency response of the postsynaptic neuron.

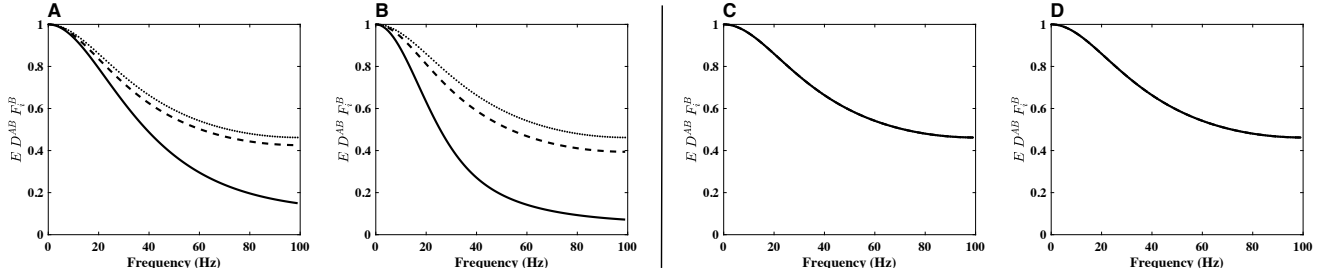


Figure 3: Frequency response of spike rate for any postsynaptic neuron i in layer B , normalised to 1, showing the impact of distance dependent propagation delays, as derived analytically in Eq. (21). Given that white noise is input to the neurons, the normalised values of the frequency response assuming no or equal delay, $F_j^B(k)$, for any postsynaptic neuron j will be 1. Therefore, only the distance-dependent propagation delay, given by $D^{AB}(k)$ for frequency k , and the postsynaptic potential, $E(k)$, impact the frequency spectra. In all figures, the solid line denotes neural response when the time constant describing propagation delay between layers, τ_l , is equal to the time constant of radial propagation delay, τ_r (Eq. (19)). The dashed line shows the case where the inter-layer delay is ten times larger than the radial propagation delay. The dotted line shows the frequency response of the postsynaptic potential function, $E(k)$. **(A,B)** Frequency responses of neurons assuming a spike velocity of $v = 10\text{ms}^{-1}$. **(C,D)** Frequency responses of neurons assuming a spike velocity of $v = 100\text{ms}^{-1}$. **(A)** Frequency responses of neurons for cell density of $7,000\text{ cells/mm}^2$, an exponential postsynaptic potential, and velocity of $v = 10\text{ms}^{-1}$. **(B)** Frequency responses of neurons for cell density of $1,000\text{ cells/mm}^2$, an exponential postsynaptic potential, and velocity of $v = 10\text{ms}^{-1}$. **(C)** Frequency responses of neurons for cell density of $7,000\text{ cells/mm}^2$, an exponential postsynaptic potential, and velocity of $v = 100\text{ms}^{-1}$. Not all lines are visible as they coincide. **(D)** Frequency responses of neurons for cell density of $1,000\text{ cells/mm}^2$, an exponential postsynaptic potential, and velocity of $v = 100\text{ms}^{-1}$. Not all lines are visible as they coincide.

3.2 Approximating the impact of propagation delay

Examination of Fig. 3 suggests that the shape of the mean propagation delay in frequency closely matches the PSP spectrum of the one-sided exponential in Fig. 3. To simplify incorporation of propagation delay into network models, we developed an approximation to the complicated Eq. (19) based on the Fourier transform of a right-sided exponential decay¹, to aid in an analytical evaluation of the impact of propagation delay. The real and imaginary components of the mean delay were modelled

¹The Fourier transform of a right-sided exponential is $\mathcal{F}[\exp(-at)u(t)] = \frac{1}{a+i\omega}$.

as a decaying sinusoid, parameterized by a decay term, τ , and a frequency term, ω , given by

$$\begin{aligned}\mathcal{R}\{D^{AB}(k)\} &= \mathcal{R}\left\{\frac{1}{1+i2\pi k\tau_D}\right\}\cos(\omega k) \\ \mathcal{I}\{D^{AB}(k)\} &= -\mathcal{R}\left\{\frac{1}{1+i2\pi k\tau_D}\right\}\sin(\omega k) \\ (D^{AB}(k))^* D^{AB}(k) &= \frac{1}{1+(2\pi k\tau_D)^2} \\ &\text{for } \omega = 2\pi\tau_l + \tau_r \\ &\text{and } \tau_D = \frac{\tau_r}{\sqrt{2}}\exp\left(-\frac{\tau_l}{2\tau_r}\right).\end{aligned}\quad (22)$$

The analytically derived impact of delay, Eq. (20), and its simpler approximation, Eq. (22), are shown in Fig. 4, verifying that the approximation is accurate across a range of inter-laminar and radial propagation delays. Minor errors are introduced at high frequencies when there is significant attenuation resulting from either comparatively long radial propagation delays, τ_r , or short delays between layers, τ_l . The error arises from slight changes in the oscillating frequency of the real and imaginary components of the mean delay across the spectrum.

The time constant that controls decay of the mean delay frequency spectrum, τ_D , decreases with increasing inter-lamina delay, τ_l , which is expected because radial delay, τ_r , becomes comparatively smaller and, therefore, propagation delay between the layers becomes more uniform. This results in less low-pass filtering of the input and retention of more high frequency components. Conversely, as the presynaptic axons become more spread out radially, the time constant that controls decay of the mean delay spectra becomes larger, resulting in increased attenuation of high frequency components. This mirrors what happens with an exponential PSP: as the time constant of a postsynaptic potential increases in the time domain, the input signal becomes increasingly smoothed and so, in the frequency domain, more of the high frequencies are attenuated.

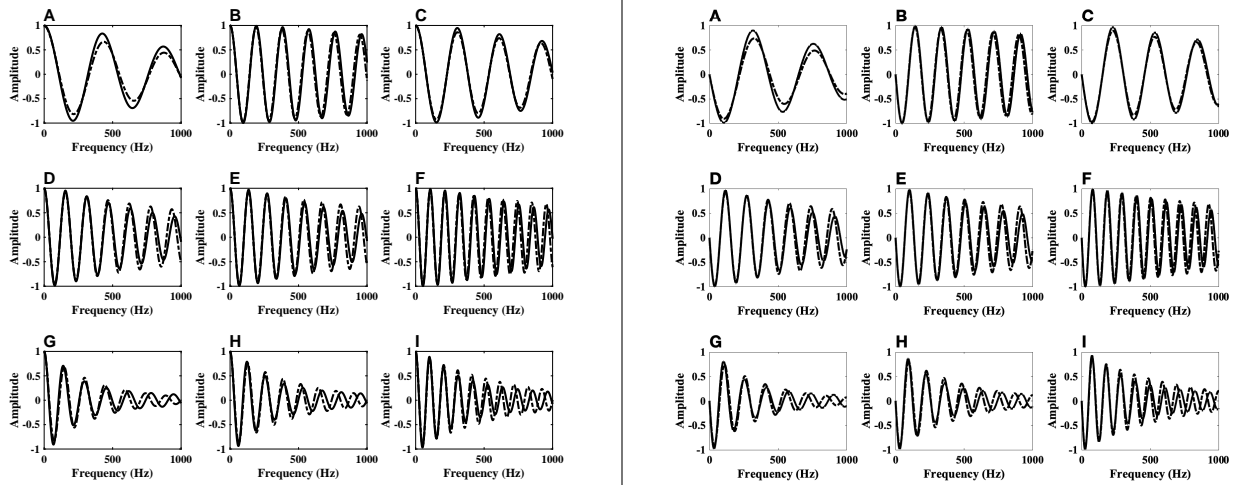


Figure 4: Approximation of the complex mean delay function, Eq. (19), describing the impact of distance-dependent propagation delay on the postsynaptic neural rate response by a decaying sinusoid, Eq. (22), for various values of inter-laminar propagation delay, τ_l , and radial propagation delay, τ_r . Real values are on the left while corresponding imaginary values are on the right. Note that the oscillation frequency of the real and imaginary components is the same. For both panels, the radial propagation delay is constant within a row, while the inter-lamina propagation delay is constant within a column, such that (A) $\tau_l = 400\mu\text{m}$, $\tau_r = 100\mu\text{m}$, (B) $\tau_l = 700\mu\text{m}$, $\tau_r = 100\mu\text{m}$, (C) $\tau_l = 900\mu\text{m}$, $\tau_r = 100\mu\text{m}$, (D) $\tau_l = 400\mu\text{m}$, $\tau_r = 200\mu\text{m}$, (E) $\tau_l = 700\mu\text{m}$, $\tau_r = 200\mu\text{m}$, (F) $\tau_l = 900\mu\text{m}$, $\tau_r = 200\mu\text{m}$, (G) $\tau_l = 400\mu\text{m}$, $\tau_r = 400\mu\text{m}$, (H) $\tau_l = 700\mu\text{m}$, $\tau_r = 400\mu\text{m}$, and (I) $\tau_l = 900\mu\text{m}$, $\tau_r = 400\mu\text{m}$.

3.3 Neural learning with propagation delay

3.3.1 Covariance of neural activity with propagation delay

In the network Linsker studied, there was equal transmission delay between neurons and rate changes were instantaneous, implying that the PSP of cells was implicitly a delta function. In this study, we develop a framework for incorporating delay and a non-trivial PSP function, and derive expressions for the covariance between layer B neurons and neural learning in synapses connecting layers B and C . This is a first step towards understanding neural learning with temporal dynamics, such as processing moving images. We assess the impact of delay and PSP function on the covariance of neurons and, hence, on the development of structure in a Linsker-type network. In order to understand how various parameters, such as propagation delay, impact the evolution of spatial opponent cells, it is necessary to derive equations for the expected size of a neuron's receptive field and the learning time constant.

Using the expression for covariance between layer B neurons, we then determine the expected receptive field size of a layer C neuron as a function of both temporal and spatial parameters. In this way, we determine the impact of propagation delay on the emerging structure of the layer C cells.

3.3.1.1 Network incorporating a general post-synaptic response To determine an expression for covariance between neurons whose activities have been filtered by a PSP kernel, Eq. (8), we extend the frequency domain expression for covariance between Poisson neurons with an implicit delta function model of the PSP, Eq. (13), to obtain

$$\begin{aligned}
\text{cov}((f_i^B \star \varepsilon), (f_j^B \star \varepsilon)) &= \frac{1}{T^2} \sum_{k=0}^T (F_i^B)^* F_j^B (E(k))^* E(k) \\
&= \frac{1}{T^2} \mathbb{E} \left[(F_i^B)^* F_j^B \right] \sum_k (E(k))^* E(k) \\
&= \text{cov}((f_i^B \star \varepsilon), (f_j^B \star \varepsilon)) \frac{\sum_k (E(k))^* E(k)}{T} \\
&= \kappa^\varepsilon \text{cov}((f_i^B \star \varepsilon), (f_j^B \star \varepsilon)), \tag{23}
\end{aligned}$$

where the second-last line follows from Eq. (7) and we have introduced κ^ε such that

$$\kappa^\varepsilon = \frac{\sum_k (E(k))^* E(k)}{T} \leq 1. \tag{24}$$

For a PSP modeled as a one-sided exponential decay function parameterized by τ_ε such that $\varepsilon = \tau_\varepsilon^{-1} \exp\left(-\frac{t}{\tau_\varepsilon}\right)$ and $(E(k))^* E(k) = \frac{1}{1+(2\pi k' \tau_\varepsilon)^2}$, lag-0 covariance evaluates to²

$$\kappa^\varepsilon = \frac{1}{2T \tau_\varepsilon}. \tag{25}$$

3.3.1.2 Network incorporating propagation delay and a general postsynaptic response We relaxed the assumption of homogeneous propagation delay for spikes from presynaptic neurons by incorporating a distance-dependent delay in the neuron model, Eq. (10). An expression for covariance between layer B neurons can be obtained by again using the frequency domain expression for covariance in Eq. (13) with respect to the spectral variates for the neuron model incorporating delay, Eq. (11),

$$\text{cov}((f_i^{B(\Delta)} \star \varepsilon), (f_j^{B(\Delta)} \star \varepsilon)) = \frac{1}{T^2} \sum_k \left(E(k) \sum_m F_m^A(k) \exp(-2\pi i \Delta_{mi} k') \right)^* E(k) \sum_n F_n^A(k) \exp(-2\pi i \Delta_{ni} k'). \tag{26}$$

²The generalised result for covariance at lag p evaluates to $\text{cov}((f_i^B \star \varepsilon)(p), (f_j^B \star \varepsilon)) = \frac{\exp\left(-\frac{p}{\tau_\varepsilon}\right)}{\tau_\varepsilon T}$

Given that the delay variables, Δ_{mi} and Δ_{ni} , are statistically independent of the layer A rate values, F_m^A and F_n^A , respectively, the inner sum terms can be separated to give

$$\begin{aligned} \text{cov}\left((f_i^{B(\Delta)} \star \varepsilon), (f_j^{B(\Delta)} \star \varepsilon)\right) &= \frac{1}{T^2} \sum_k (E(k))^* E(k) \left(\mathbb{E} \left[\exp(-2\pi i \Delta_{mi} k') \right] \right)^* \mathbb{E} \left[\exp(-2\pi i \Delta_{ni} k') \right] \left(\sum_m F_m^A(k) \right)^* \sum_n F_n^A(k) \\ &= \frac{1}{T^2} \sum_k (E(k))^* E(k) \left(\mathbb{E} \left[\exp(-2\pi i \Delta_{mi} k') \right] \right)^* \mathbb{E} \left[\exp(-2\pi i \Delta_{ni} k') \right] (F_i^B(k))^* F_j^B(k). \end{aligned} \quad (27)$$

Using the expected value of delay denoted by $D^{AB}(k) = \mathbb{E} \left[\exp(-2\pi i \Delta k') \right]$ and given in Eq. (20), covariance between layer B neurons in the presence of delay and a PSP can be expressed as

$$\begin{aligned} \text{cov}\left((f_i^{B(\Delta)} \star \varepsilon), (f_j^{B(\Delta)} \star \varepsilon)\right) &= \frac{1}{T^2} \sum_k (E(k))^* E(k) (D^{AB}(k))^* D^{AB}(k) (F_i^B(k))^* F_j^B(k) \\ &= \frac{1}{T^2} \sum_k (E(k))^* E(k) (D^{AB}(k))^* D^{AB}(k) (F_i^B(k))^* F_j^B(k) \\ &= \text{cov}(f_i^B, f_j^B) \frac{\sum_k (E(k))^* E(k) (D^{AB}(k))^* D^{AB}(k)}{T} \\ &= \kappa_{\Delta}^{AB} \text{cov}(f_i^B, f_j^B), \end{aligned} \quad (28)$$

where κ_{Δ}^{AB} expresses the attenuation of covariance in neural activity between postsynaptic neurons in layer B resulting from propagation delay between layers A and B , and is defined by

$$\kappa_{\Delta}^{AB} = \frac{\sum_{k=0}^T (D^{AB}(k))^* D^{AB}(k) (E(k))^* E(k)}{T} \leq 1. \quad (29)$$

For a PSP modelled as a one-sided exponential decay parameterized by τ_{ε} , this evaluates to

$$\kappa_{\Delta}^{AB} = \frac{\tau_{\varepsilon} - \tau_D}{2T(\tau_{\varepsilon}^2 - \tau_D^2)}, \quad (30)$$

where τ_D is determined from the propagation delay between layers, τ_l , and the radial propagation delay, τ_r , according to the approximation in Eq. (22)³. Note that, if propagation delay is assumed to be 0, this reduces to the network incorporating a PSP-only case detailed in Eq. (24).

Fig. 5 shows correlation between layer B neurons for Linsker's (1986a) network, for a network incorporating a non-trivial postsynaptic potential, and for a network incorporating both distance-dependent propagation delay and a non-trivial postsynaptic potential. Fig. 5B shows that, for a network with no propagation delay, an exponentially decaying postsynaptic potential spreads the impact of each spike over time, which does not impact expected correlation when there is no propagation delay. This is intuitive for white input; however, the correlation matrix is noisier, reflecting the increased variance in sample correlation owing to the loss of signal power in the input after low pass filtering (Davey et al., 2013).

Fig. 5C shows the impact of propagation delay when a trivial delta function postsynaptic potential is used. Propagation delay spreads out the arrival of spikes to the neuron but, since the spikes are instantaneous, the majority of correlation between layer B neurons is destroyed. Finally, Fig. 5D shows that, while propagation delay spreads out the arrival times of spikes to layer B postsynaptic neurons, the postsynaptic potential spreads the impact of each spike out over time, mitigating the impact of propagation delay. Note that the correlation matrix is also noisy because the sample variance of correlation increases from the low-pass filtering.

³Note that for lagged covariance this more generally evaluates to $\text{cov}\left((f_i^{B(\Delta)} \star \varepsilon)(p), (f_j^{B(\Delta)} \star \varepsilon)\right) = \kappa_{\Delta}^{AB}(p) \text{cov}(f_i^B, f_j^B)$, where $\kappa_{\Delta}^{AB}(p) = \frac{\exp\left(-\frac{p}{\tau_{\varepsilon}}\right) \tau_{\varepsilon} - \exp\left(-\frac{p}{\tau_D}\right) \tau_D}{2(\tau_{\varepsilon}^2 - \tau_D^2)}$ for a lag of p .

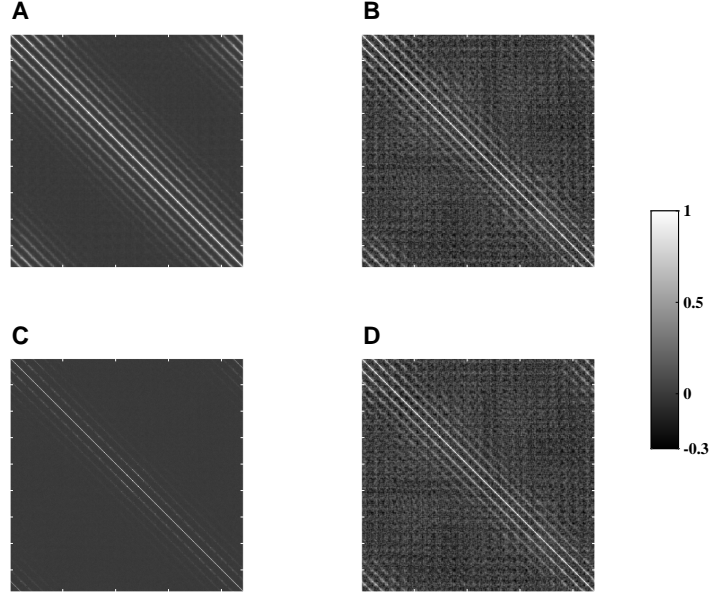


Figure 5: Normalised covariance between layer B neurons with and without incorporating distance-dependent propagation delay. The additional correlation on the off diagonal edges reflects the periodic boundaries used in simulations to avoid edge artifacts. Each axis is neuron index in the layer. **(A)** Correlations between layer B neurons for Linsker’s (1986a) network, Eq. (12). **(B)** Correlations between layer B neurons for a network with postsynaptic potential modelled by an exponential decay with a 10ms time constant, Eq. (23). **(C)** Correlations between layer B neurons for a network with distance-dependent propagation delay and a trivial delta function model for the postsynaptic potential, Eq. (28). **(D)** Correlations between layer B neurons for a network with distance-dependent propagation delay and a postsynaptic potential modelled by an exponential decay with a 10ms time constant, Eq. (28).

3.3.2 Learning equation with propagation delay

Thus far, we have derived the covariance between the neural activities of layer B neurons. However, when these neurons propagate spikes to a postsynaptic layer C neuron, there will be a delay as the signal propagates from layer B to layer C , where arrival at the postsynaptic neuron will cause the signal to be further filtered by PSP of the postsynaptic cell. To evaluate the impact of this, it is necessary to consider the origin of the learning rule in Eq. (14b), outlined in Eq. (14b), in the context of the presynaptic output being delayed before arriving at the synapse where learning occurs, and the postsynaptic neural activity being filtered again at the layer C site. Using the model for layer C neural activity given in Eq. (10b) and assuming that the plasticity process of synapse weight change is initiated near the cell body of the post-synaptic neuron, the learning equation becomes

$$w_{ip}^{BC} = \eta \left(k_1^{BC} + \frac{1}{N^{BC}} \sum w_{jp}^{BC} \left(Q \left((f_j^{B(\Delta)} \star \varepsilon) (t - \Delta_{jp}^{BC}), (f_i^{B(\Delta)} \star \varepsilon) (t - \Delta_{ip}^{BC}) \right) + k_2^{BC} \right) \right), \quad (31)$$

where Q is the normalized form of covariance between layer B neurons.

To evaluate this covariance in the presence of propagation delay and arbitrary PSP, we can use the framework established in Section 3.3.1.2. Application of the result in Eq. (28) to calculate covariance between layer B output and layer C input, and

using $D^{AB}(k)$ from Eq. (18), we obtain

$$\begin{aligned}
& \text{cov} \left((f_j^{B(\Delta)} \star \varepsilon) (t - \Delta_{jp}^{BC}), (f_i^{B(\Delta)} \star \varepsilon) (t - \Delta_{ip}^{BC}) \right) \\
&= \frac{1}{T^2} \sum_k \left(E(k) \exp(-2\pi i \Delta_{jp}^{BC} k') \sum_n F_n^A(k) \exp(-2\pi i \Delta_{nj}^{AB} k') \right)^* E(k) \exp(-2\pi i \Delta_{ip}^{BC} k') \sum_m F_m^A(k) \exp(-2\pi i \Delta_{mi}^{AB} k') \\
&= \frac{1}{T^2} \sum_k (E(k))^* E(k) (D^{AB}(k))^* D^{AB}(k) \exp(-2\pi i k' (\Delta_{ip}^{BC} - \Delta_{jp}^{BC})) (F_i^B(k))^* F_j^B(k) \\
&= \text{cov} (f_i^B, f_j^B) \frac{1}{T} \sum_k (E(k))^* E(k) (D^{AB}(k))^* D^{AB}(k) \exp(-2\pi i k' (\Delta_{ip}^{BC} - \Delta_{jp}^{BC})) \\
&= \kappa_{\Delta_{ij}}^{BC} \text{cov} (f_i^B, f_j^B), \tag{32}
\end{aligned}$$

where $\kappa_{\Delta_{ij}}^{BC}$ captures attenuation of covariance in activity of layer B presynaptic neurons i and j on arrival at the postsynaptic neuron in layer C by propagation delay between both layers A and B and layers B and C . Propagation delay is compounded from the input layer A all the way to layer C because covariance is induced by common synapses from layer A to layer B neurons.

Eq. (32) describes the expected covariance between inputs arriving from two layer B neurons, i and j , at the synapse of a given layer C cell, p , taking into consideration distance-dependent axonal propagation delays. Therefore, the result depends on the position of the layer B presynaptic neurons relative to the layer C postsynaptic neuron p . More precisely, the result depends on the difference in spike arrival times between neuron i and neuron j at the neuron p in layer C , given by $\Delta_{ip}^{BC} - \Delta_{jp}^{BC}$, which itself is a function of the radial distance between i and j , the interlaminar distance between layers B and C , and the spike propagation velocity; i.e., $\Delta_{ip}^{BC} - \Delta_{jp}^{BC} = \frac{((d_{ip}^B)^2 + (d^{BC})^2)^{\frac{1}{2}} - ((d_{jp}^B)^2 + (d^{BC})^2)^{\frac{1}{2}}}{v}$. This has the effect of further attenuating covariance between the presynaptic layer B neurons because, if the difference in spike arrival times is not within the smoothing period of the PSP, the covariance is destroyed.

To analytically examine the impact of propagation delay on learning, we use the decaying sinusoidal approximation of the real and imaginary components of mean delay in the frequency spectrum, which results in a frequency spectrum of $(D^{AB}(k))^* D^{AB}(k)$ that is well approximated by $\frac{1}{1+(2\pi k' \tau_D)^2}$ (see Eq. (22)). We also introduce a simple one-sided exponential PSP such that $\varepsilon = \frac{1}{\tau_\varepsilon} \exp\left(-\frac{t}{\tau_\varepsilon}\right)$ and $(E(k))^* E(k) = \frac{1}{1+(2\pi k' \tau_\varepsilon)^2}$. Therefore, we can write the expression for attenuation of covariance between inputs from B neurons, i and j , arriving at the postsynaptic neuron, Eq. (32), as

$$\begin{aligned}
\kappa_{\Delta_{ij}}^{BC} &= \sum_{k=0}^T \frac{1}{\left(1+(2\pi k' \tau_D)^2\right)} \frac{1}{\left(1+(2\pi k' \tau_\varepsilon)^2\right)} \exp(-2\pi i k' (\Delta_{ip}^{BC} - \Delta_{jp}^{BC})) \\
&= \frac{\exp\left(-\Delta_{ij} \frac{\tau_\varepsilon + \tau_D}{\tau_\varepsilon \tau_D}\right) \left(\exp\left(\frac{\Delta_{ij}}{\tau_D}\right) \tau_\varepsilon - \exp\left(\frac{\Delta_{ij}}{\tau_\varepsilon}\right) \tau_D\right)}{2(\tau_\varepsilon - \tau_D)(\tau_\varepsilon + \tau_D)} \tag{33}
\end{aligned}$$

for lag-0 covariance⁴ and for $\Delta_{ij} = \left| \Delta_{ip}^{BC} - \Delta_{jp}^{BC} \right|$. For the case of zero propagation delay, this reduces to the covariance between neurons in the presence of propagation delay only, Eq. (25).

The rate of change of synaptic weights between layers B and C can then be given as

$$\dot{w}_{ip}^{BC} \triangleq \eta \langle (\Delta_{ij} w_{ip}) \rangle = \eta \left(k_1^{BC} + \frac{1}{N_{BC}} \sum w_{jp}^{BC} \left(\kappa_{\Delta_{ij}}^{BC} Q(f_j^B, f_i^B) + k_2^{BC} \right) \right). \tag{34}$$

The receptive fields in a three-layer Linsker (1986a) model are well known to evolve into spatial opponent cells. Since attenuation of covariance from propagation delay is circularly symmetric, we do not expect the shape of the resulting receptive fields to change. However, we examine properties such as the size of the on-centre in the resulting spatial opponent cell and time to convergence for synaptic weights.

⁴For lagged covariance this result generalises to $\text{cov} \left((f_j^{B(\Delta)} \star \varepsilon) (t - (\Delta_{jp}^{BC} - p)), (f_i^{B(\Delta)} \star \varepsilon) (t - \Delta_{ip}^{BC}) \right) = \frac{\exp\left(-(\Delta_{ij} + p) \frac{\tau_\varepsilon + \tau_D}{\tau_\varepsilon \tau_D}\right) \left(\exp\left(\frac{(\Delta_{ij} + p)}{\tau_D}\right) \tau_\varepsilon - \exp\left(\frac{(\Delta_{ij} + p)}{\tau_\varepsilon}\right) \tau_D\right)}{2(\tau_\varepsilon - \tau_D)(\tau_\varepsilon + \tau_D)}$, for lag p .

3.4 On-center size

For cortical neurons, the term ‘receptive field’ is assumed to refer to an inter-layer receptive field, defined by a cortical neuron’s input synaptic weight structure. We wish to analytically derive an expression for the size of the on-center of a neuron’s receptive field to determine the impact of propagation delay on the evolution of layer C spatial-opponent neurons. To this end, we consider the neuron when it has undergone sufficient learning (see the learning equation, Eq. (14b)) such that the weights of all synapses connecting to the layer C neuron have diverged to the upper or lower bound. This assumption is valid because the learning equation is unstable and, hence, all weights, or all but one, will reach a stable limiting value (see Linsker (1986a), p. 7510).

3.4.1 Linsker’s network

To determine the size of a neuron’s on-center, it is necessary to determine its average synaptic weight. We assume that synaptic weights are independent of covariance between neural output early in the learning process. The mean weight converges during this early stage (Kempster et al., 1999) and, thus, from Eq. (14b), we can write

$$\dot{w}^{BC} = \eta \left(k_1^{BC} + \bar{w}^{BC} \left(k_2^{BC} + \overline{Q^{BB}} \right) \right), \quad w_{\min}^{BC} \leq \bar{w}^{BC} \leq w_{\max}^{BC}, \quad (35)$$

where \bar{w}^{BC} denotes the mean weight of synapses between layer B and layer C and $\overline{Q^{BB}}$ is the mean covariance between layer B neural outputs. As noted by Linsker (1986a), for $k_2^{BC} > 0$, the weights are unstable and grow to the bounds. Linsker (1986a) showed that k_2^{BC} can be derived from first-order firing rate statistics and is positive if the postsynaptic neuron is firing at a rate that is greater than a given constant benchmark rate, and vice-versa. This means that, for the mean weight to be stable, the mean rate of neural firing must be less than this benchmark value.

The fixed point for the mean weight follows immediately,

$$\bar{w}_*^{BC} = \frac{-k_1^{BC}}{k_2^{BC} + \overline{Q^{BB}}}. \quad (36)$$

To determine the fixed point for the mean weight, we need to calculate the mean covariance between layer B neurons. As per Linsker (1986a), we normalize the temporal covariance between layer B neurons by dividing by input variance and number of input connections (Eqs. (15) and (16)). Consequently, for the case of a delta function PSP and instantaneous propagation delay, the covariance of a neuron with itself is 1. The average covariance between layer B neurons can now be found by integrating covariance over the laminar (see Appendix F for details),

$$\begin{aligned} \overline{Q^{BB}} &= \frac{1}{(\pi(\sigma^{BC})^2)^2} \int_{-\infty}^{\infty} \int_{-\infty}^{\infty} \exp\left(-\frac{|\mathbf{x}^2 - \mathbf{x}'^2|}{2(\sigma^{AB})^2}\right) \exp\left(-\frac{\mathbf{x}^2}{(\sigma^{BC})^2}\right) \exp\left(-\frac{\mathbf{x}'^2}{(\sigma^{BC})^2}\right) d\mathbf{x}' d\mathbf{x} \\ &= \frac{1}{1 + \frac{(\sigma^{BC})^2}{(\sigma^{AB})^2}}. \end{aligned} \quad (37)$$

From Eq. (37), it can be seen that mean covariance between layer B neurons is maximized by either maximizing the connection radius between layers A and B or minimizing the connection radius between layers B and C .

Now it is necessary to calculate the average weight of a layer C synapse with receptive field size of r_{on} . Knowing that synapses within the on-center have reached the upper limiting value of w_{\max}^{BC} while synapses outside of it have reached the lower limiting value of w_{\min}^{BC} , we can determine the average synaptic weight by integrating individual synapse weights scaled by the probability of each synapse being connected to the layer C neuron. Implementing the integral in polar coordinates this time, we obtain

$$\begin{aligned} \bar{w}_*^{BC} &= \frac{w_{\max}^{BC}}{\pi(\sigma^{BC})^2} \int_0^{r_{\text{on}}} \int_0^{2\pi} \exp\left(-\frac{\tilde{r}^2}{(\sigma^{BC})^2}\right) d\tilde{r} d\tilde{\theta} - \frac{w_{\min}^{BC}}{\pi(\sigma^{BC})^2} \int_{r_{\text{on}}}^{\infty} \int_0^{2\pi} \exp\left(-\frac{\tilde{r}^2}{(\sigma^{BC})^2}\right) d\tilde{r} d\tilde{\theta} \\ &= w_{\max}^{BC} \left(1 - \exp\left(-\frac{(r_{\text{on}})^2}{(\sigma^{BC})^2}\right) \right) + w_{\min}^{BC} \left(\exp\left(-\frac{(r_{\text{on}})^2}{(\sigma^{BC})^2}\right) \right). \end{aligned} \quad (38)$$

For a lower weight bound of 0 and an upper weight bound of 1, this gives

$$\overline{w}_*^{BC} = 1 - \exp\left(-\frac{(r_{\text{on}})^2}{(\sigma^{BC})^2}\right). \quad (39)$$

Finally, to determine the size of the on-center as a function of covariance, equate the two equations for mean synaptic weight, Eqs. (36) and (38), and rearrange to obtain

$$r_{\text{on}} = \sigma^{BC} \sqrt{\log\left(\frac{k_2^{BC} + \overline{Q}^{BB}}{w_{\text{max}}^{BC} (k_2^{BC} + \overline{Q}^{BB}) + k_1^{BC}}\right)} \quad (40)$$

$$= \sigma^{BC} \sqrt{\log\left(\frac{1}{w_{\text{max}}^{BC} - \overline{w}_*^{BC}}\right)}, \quad (41)$$

where we have used the assumption that $w_{\text{max}}^{BC} - w_{\text{min}}^{BC} = 1$ (Linsker, 1986a) and applied the equation for the fixed point to go from Eq. (40) to Eq. (41). Note that, since the numerator of Eq. (40) must be negative for the mean weight to be stable (see Eq. (35)), the denominator must also be negative for the size of the on-center to be a real number.

3.4.2 Network incorporating a general post-synaptic response

To calculate receptive field size for a network with an arbitrary PSP and identical propagation delays between all neurons, Eq. (40) can be trivially extended to the case for which an arbitrary PSP is incorporated into the neuron model since the impact of the PSP on covariance is to scale it by a constant factor, Eq. (23). Consequently, the expected size of a layer C neuron's receptive field becomes

$$r_{\text{on}}^\varepsilon = \sigma^{BC} \sqrt{\log\left(\frac{k_2^{BC} + \kappa^\varepsilon \overline{Q}^{BB}}{w_{\text{max}}^{BC} (k_2^{BC} + \kappa^\varepsilon \overline{Q}^{BB}) + k_1^{BC}}\right)}. \quad (42)$$

3.4.3 Network incorporating propagation delay and a general post-synaptic response

We now determine expressions for the receptive field size for an arbitrary PSP function and propagation delay that is proportional to the three-dimensional distance between neurons. Using these expressions, a neuron's receptive field size will be calculated in this more realistic context.

Introduce the term, $\delta_{\Delta, \varepsilon}^{BC} = vd^{BC}\tau_\varepsilon$, which captures the elements that minimize the spread in arrival time of input spikes to the layer C post-synaptic neuron. As inter-layer distance, d^{BC} , and velocity, v , increase, the impact of radial propagation delay decreases because there is reduced spread in arrival times of spikes that were initiated simultaneously in layer B . As the PSP time constant, τ_ε , increases, the impact of radial propagation delay is reduced because the input signals are low-pass filtered.

Using the expressions for covariance derived in Section 3.3.1, the average covariance into a layer C cell when propagation delay and PSP are incorporated are found to be (see Section F.2 for details)

$$\begin{aligned} \overline{Q}_{\Delta, \varepsilon}^{BB} = & \frac{1}{(\tau_\varepsilon - \tau_D)^2 (\tau_\varepsilon + \tau_D)^2} \left(\frac{4 \left(2 + \frac{(\sigma^{BC})^2}{(\sigma^{AB})^2}\right) \tau_\varepsilon^2}{\left(\frac{(\sigma^{BC})^2}{vd^{BC}\tau_\varepsilon} - 2\right) \left(\frac{(\sigma^{BC})^2}{vd^{BC}\tau_\varepsilon} - 2 - 2\frac{(\sigma^{BC})^2}{(\sigma^{AB})^2}\right) \left(\frac{(\sigma^{BC})^2}{vd^{BC}\tau_\varepsilon} + 2 + \frac{(\sigma^{BC})^2}{(\sigma^{AB})^2}\right)} \right. \\ & \left. + \frac{4 \left(2 + \frac{(\sigma^{BC})^2}{(\sigma^{AB})^2}\right) \tau_D^2}{\left(\frac{(\sigma^{BC})^2}{vd^{BC}\tau_D} - 2\right) \left(\frac{(\sigma^{BC})^2}{vd^{BC}\tau_D} - 2 - 2\frac{(\sigma^{BC})^2}{(\sigma^{AB})^2}\right) \left(\frac{(\sigma^{BC})^2}{vd^{BC}\tau_D} + 2 + \frac{(\sigma^{BC})^2}{(\sigma^{AB})^2}\right)} \right). \end{aligned} \quad (43)$$

Note that this result is undefined for $\tau_\varepsilon = \tau_D$ and, for zero propagation delay and a long inter-laminar distance, this reduces to the same attenuation as for a network with an exponential PSP, $\kappa^\varepsilon \overline{Q}^{BB}$.

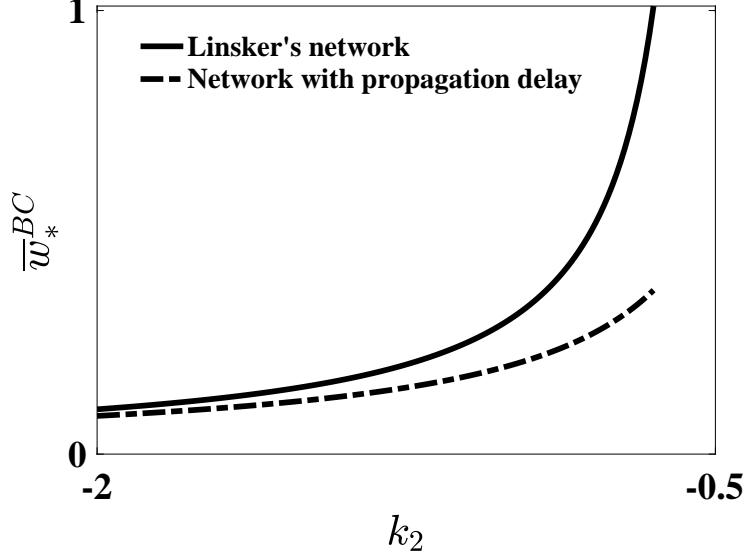


Figure 6: Fixed point mean weight for Linsker's (1986a) network (Eq. (36), solid line) compared to the fixed point mean weight for the network incorporating propagation delay and an arbitrary PSP (Eq. (46), dot-dashed line). The figure was generated with $k_1^{BC} = -0.5 \text{ s}^{-1}$ and $\overline{Q}^{BB} = 0.5 \text{ s}^{-1}$, Eq. (37). Mean covariance for the network with delay was $\overline{Q}_{\Delta,\varepsilon}^{BB} = 0.24 \text{ s}^{-1}$, Eq. (43), calculated from $\tau_\varepsilon = 1 \text{ mm}^2$, $\tau_D = 0.1 \text{ mm}^2$, $(\sigma^{AB})^2 = 100$ grid spaces, $(\sigma^{BC})^2 = 200$ grid spaces, $d^{BC} = 400$ grid spaces, and $v = 10 \text{ m/s}$.

The impact of delay from propagation between layers is to attenuate covariance, so that $\overline{Q}_{\Delta,\varepsilon}^{BB} \leq \overline{Q}^{BB}$. Attenuation resulting from delay between layers A and B is captured in κ_{Δ}^{AB} , which is itself a function of radial propagation delay, τ_r , and inter-laminar propagation delay, τ_l . For delay between layers B and C , this is captured by the relationship between σ^{BC} and $vd^{BC}\tau_D$ (velocity, distance between the layers and the time constant of propagation delay) such that the larger the connectivity radius, the larger the denominator and the more covariance is attenuated. The radial propagation delay spreads out the arrival time in every consecutive layer pair, compounding the impact of radial delay.

Importantly, for large inter-laminar delay, mean covariance in the presence of propagation delay approaches mean covariance in Linsker's (1986a) network, Eq. (37), since the impact of radial propagation delay becomes negligible, such that

$$\overline{Q}_{\Delta,\varepsilon}^{BB} \stackrel{d^{BC} \rightarrow \infty}{\approx} \frac{1}{1 + \frac{(\sigma^{BC})^2}{(\sigma^{AB})^2}}. \quad (44)$$

The mean synapse weight converges in the early stages of learning, having a much faster time constant than that of the individual synapses (Kempster et al., 1999). The learning equation for the mean weight synapse in the presence of propagation delay can be expressed as

$$\dot{\overline{w}}^{BC} = \eta \left(k_1^{BC} + \overline{w}^{BC} \left(k_2^{BC} + \overline{Q}_{\Delta,\varepsilon}^{BB} \right) \right), \quad w_{\min}^{BC} \leq \overline{w}^{BC} \leq w_{\max}^{BC}, \quad (45)$$

so that

$$\overline{w}_*^{BC} = \frac{-k_1^{BC}}{k_2^{BC} + \overline{Q}_{\Delta,\varepsilon}^{BB}}. \quad (46)$$

Consequently, the fixed point of the mean weight is modified by the impact of propagation delay. Since the denominator is negative and $k_2^{BC} < 0$, reducing the size of the mean covariance decreases the size of the mean weight to which the network converges.

Fig. 6 shows a comparison of the fixed point mean synapse weight for Linsker's (1986a), Eq. (37), and the network incorporating propagation delay and arbitrary ε , Eq. (46). Large changes in the homeostatic constant, k_2^{BC} , result in relatively small

changes in the fixed point mean weight for the network with propagation delay. In contrast, the same change in homeostatic constant causes the mean weight in Linsker’s (1986a) network to change from a value near the lower weight bound to a value to the upper weight bound.

The expected receptive field size after incorporating both propagation delay and an arbitrary PSP function is

$$r_{\text{on}}^{\Delta, \epsilon} = \sigma^{BC} \sqrt{\log \left(\frac{k_2^{BC} + \overline{Q_{\Delta, \epsilon}^{BB}}}{w_{\text{max}}^{BC} (k_2^{BC} + \overline{Q_{\Delta, \epsilon}^{BB}}) + k_1^{BC}} \right)} \quad (47)$$

$$= \sigma^{BC} \sqrt{\log \left(\frac{1}{w_{\text{max}}^{BC} - \overline{w}_*^{BC}} \right)}. \quad (48)$$

This equation shows that receptive field size depends on the mean covariance, $\overline{Q_{\Delta, \epsilon}^{BB}}$, which was derived to be a function of the radial versus inter-laminar propagation delays and the PSP decay time constant. The fixed point mean weight is more stable for the network with propagation delay and, therefore, the range in receptive field sizes will also be smaller. Consequently, propagation delay has the effect of limiting the impact of correlation from distal neurons, which stabilises the fixed point mean weight and receptive field sizes.

4 Discussion

Linsker (1986a) proposed a simple rate-based, three-layer, feed-forward network to show how spatial opponent cells emerge after a period of learning based purely on spontaneous activity and in the absence of external environmental input. Linsker (1986a) demonstrated that Gaussian distributed synaptic connectivity between the layers was sufficient to introduce spatially-dependent correlation in neural outputs, which in turn prompted a self-organizing network. MacKay and Miller (1990) provided a mathematical framework from which to study Linsker’s (1986a) network, while Wimbauer et al. (1998) extended the analysis to include lateral connectivity in the third layer. While these works were formative in establishing a possible mechanism underlying synaptic learning of simple cells prior to birth, they assumed that propagation delay between all neurons was identical and, consequently, had negligible impact.

In this study the assumption of identical propagation delays in Linsker’s (1986a) network, introducing delays that account for both radial distance (i.e., separation within the lamina) and inter-laminar distance (i.e., separation between the layers) is relaxed. The results demonstrate that the impact of propagation delay is to attenuate high frequency information in the neural activity. This is intuitive since propagation delay spreads out the arrival time of input to the neurons: when the inputs are summed together as they arrive at the postsynaptic neuron, the spread in arrival times filters out the high frequency components of the signal. As the impact of radial propagation delay increases by enlarging the synaptic connectivity radius, reducing neuron density, reducing propagation velocity, or reducing the inter-laminar distance, the spread in signal arrival times from the previous layer becomes more dispersed and the higher frequencies are increasingly attenuated. Consequently, propagation delay acts as a low-pass filter, where the cut-off frequency is determined by the relationship of the radial propagation delay to the inter-laminar propagation delay. Our results demonstrate that the ratio of inter-laminar propagation delay to within layer, radial propagation delay, is the crucial factor in determining the extent of the low-pass filtering. To facilitate the application of our results to analytical models of learning, we derived a simplified model of the impact of propagation delay using an effective delay time constant, determined from the inter-laminar propagation delay and the radial propagation delay.

A general post-synaptic potential (PSP) with a finite time course was introduced, which was interpreted as spreading the probability of a spike over a finite period and thus low-pass filtering the input. The values of the PSP time constants were chosen to reflect the effective membrane time constant, which is shorter than the passive membrane time constant due to the neuron becoming more leaky as more synaptic channels open with increased activity (Burkitt et al., 2003). Where the PSP has a lower cut-off frequency than the effective cut-off frequency imposed by propagation delay, differences in the synaptic connectivity radius and inter-laminar distance had negligible effect on the frequency spectra of the postsynaptic neuron’s activity. Consequently, differences in neural activity resulting from propagation delay became minimal in these circumstances. Thus, the PSP can play an important role in standardising the frequency spectra of neural activity in the presence of differing propagation delay properties amongst neurons. Conversely, where propagation delay has a longer effective time constant than that of the PSP and, therefore, a lower cut-off frequency, propagation delay can significantly attenuate frequencies that are present after convolution with the PSP. Therefore, the effective time constant of each enables the processing of similar scales

of temporal information. These results can apply to any topographical multi-layered network, and is seen in the retina, where time constants at the periphery have been found to be up to twice as long as those in the fovea, where neurons are much more densely packed (Sinha et al., 2017).

Linsker (1986a) showed that, under Gaussian synaptic connectivity distributions, covariance between firing rates of two neurons in the second layer is a Gaussian function of their radial separation distance in the lamina. In this study we showed that, when distance-dependent propagation delay between the first and second layers is considered and there is a more biophysically realistic PSP, covariance between the outputs of neurons in the second layer can be expressed as a scaled function of covariance between neurons in Linsker’s (1986a) network. That is, when propagation delay and PSP are accounted for, covariance between two neurons in the second layer remains a Gaussian function of their separation distance in the lamina, but is attenuated by a constant determined by the mean propagation delay between the first and second layers and the PSP function. The PSP was found to be important because, in its absence, if two presynaptic neurons at different distances from the postsynaptic neuron were instantaneously correlated, propagation delay reduced the correlation, since the activity from the two neurons arrived at the postsynaptic neurons at different times. Thus, the PSP plays a crucial role in enabling correlation at non-zero lags to be incorporated in the output of a postsynaptic neurons.

The change in frequency content of the summed input to a postsynaptic neuron as radial propagation delay becomes more prominent may explain some experimental results in the visual system. In the visual system, it has been found that contrast sensitivity is frequency dependent in the periphery, with sensitivity decreasing for higher frequencies (Venkataraman et al., 2017). This accords with our results, since neurons that are more spread out receive input that is attenuated at higher frequencies and thus higher amplitude input is required to obtain a similar response. Additionally, Thibos et al. (1996) demonstrated that cut-off frequency is a function of eccentricity, decreasing as distance from the fovea increases. This likewise accords with our results: as the impact of radial delay increases with distance from the fovea, delay acts like a low-pass filter, where the cut-off frequency decreases as neurons become more spread across the lamina.

A further contribution of this paper was to consider the size of the on-center of the spatial opponent neuron that emerges in the third layer. This was determined by calculating the fixed point for the mean synaptic weight and establishing how large the on component was required to be in order to establish the fixed point mean weight. The learning equation for the mean weight is stable only when the competitive plasticity component is negative and larger in magnitude than the non-competitive component. The competitive component comprises a negative constant and the positive mean covariance between the presynaptic inputs. If the mean covariance approaches the magnitude of the negative constant in magnitude, the fixed-point weight becomes increasingly large until it reaches a point of instability. Furthermore, as the fixed-point weight approaches the upper weight bound, the size of the neuron’s on-center increases rapidly.

When propagation delay is incorporated into the network, the fixed point weight, and hence the on-center size of the spatial opponent neuron, is much more stable to changes in homeostatic parameters and factors that determine covariance. A small change in the homeostatic constant parameters (k_1, k_2) can trigger a large change in the fixed point weight in Linsker’s (1986a) network and, hence, a large change in the receptive field structure of the cell. The fixed-point weight for the network with propagation delay is comparatively stable. The region of instability for Linsker’s (1986a) is largely avoided since covariance is attenuated, and so the fixed point weight does not approach the upper bound.

The results of this study show that a small connectivity radius in addition to densely packed cells, and consequently negligible radial propagation delay, both act to maintain large covariances between presynaptic inputs. The consequence of this is a larger mean synaptic weight and comparatively larger on-center spatial extent. Therefore, densely packed cells with small connectivity radii have mostly excitatory input and very little inhibitory input. Conversely, cells that are more spread out and more likely to connect to neurons further away have a smaller mean synaptic weight, which results in a smaller on-center. Therefore, these neurons have more inhibitory input. Interestingly, Sun et al. (2007) found that, in human primary visual cortex (V1), cells responding to high spatial frequency preferred low speed input, while cells responding to low spatial frequency preferred high speed input, similar to what is found in cats (Shoham et al., 1997). Our results provide a potential explanation for this finding, in that simple cells preferring low spatial frequency input have a larger on-centre, requiring a higher mean covariance of presynaptic inputs, which in turn requires high speed input so that presynaptic spikes are arrival times are not too spread out.

Finally, although we assume here that axonal propagation dominates spike delay, our results nevertheless generalise to the case in which dendrite propagation dominates delay, as the analytical results remain unchanged, but the additional delay between layers two and three is not required in the learning equation, simplifying the result.

Acknowledgements

The authors acknowledge support under the Australian Research Council's Discovery Projects funding scheme (Project DP140102947). CED acknowledges support of a University of Melbourne Research Fellowship.

Appendix

Appendix A Expected number of shared inputs

To examine network dynamics, it is necessary to ascertain the expected number of shared connections between two neurons. The number of shared connections from a presynaptic layer to two neurons in the postsynaptic layer, say i and j , depends on the radial distance between them since the synaptic connection density for each is a Gaussian function of distance (see Fig. 1). We assume for simplicity and without loss of generality that i and j differ only in their x coordinate so that $d_{ij}^B = x_{mi} - x_{mj}$.

Center the Cartesian coordinates describing a neuron's position in the lamina on one of the postsynaptic neurons, say i , so that the other postsynaptic neuron, say j , lies on the x axis. From Eq. (1), neuron, m , in layer A , has a probability of connecting to neuron i in layer B of $p_N(x_{mi}, y_{mi}; \mathbf{0}, \Sigma^A)$ and a probability of connecting to neuron j in layer B of $p_N(x_{mj}, y_{mj}; \mathbf{0}, \Sigma^A) = p_N(x_{mi} - d_{ij}^B, y_{mi}; \mathbf{0}, \Sigma^A)$. The probability of the presynaptic neuron connecting to both postsynaptic neurons i and j is simply the product of the probability of each individual connection being made. The expected number of common connections can be determined by summing this joint probability over the layer or, in the continuous limit, integrating the joint probability over the layer of presynaptic neurons. If N^{AB} denotes the number of synaptic connections from layer A to a layer B neuron and $N^{BB}(d)$ the number of shared connections between two postsynaptic neurons in layer B separated by a distance of d , then in the continuous limit,

$$N^{BB}(d) = (N^{AB})^2 \iint_{xy} p_N(x, y; \mathbf{0}, \Sigma^A) p_N(x-d, y; \mathbf{0}, \Sigma^A) dx dy, \quad (49)$$

where the sub- and super-scripts on distance parameters have been dropped to aid readability. This can be expanded as

$$\begin{aligned} N^{BB}(d) &= (N^{AB})^2 \iint_{xy} \frac{1}{(\pi(\sigma^{AB})^2)^2} \exp\left(-\frac{x^2 + y^2}{(\sigma^{AB})^2}\right) \exp\left(-\frac{(x-d)^2 + y^2}{(\sigma^{AB})^2}\right) dx dy \\ &= \frac{(N^{AB})^2}{(\pi(\sigma^{AB})^2)^2} \iint_{xy} \exp\left(-\frac{2x^2 + 2y^2 + d^2 - 2xd}{(\sigma^{AB})^2}\right) dx dy \\ &= \frac{(N^{AB})^2}{(\pi(\sigma^{AB})^2)^2} \iint_{xy} \exp\left(-\frac{2\left(\left(x - \frac{d}{2}\right)^2 + y^2 + \frac{d^2}{4}\right)}{(\sigma^{AB})^2}\right) dx dy. \end{aligned} \quad (50)$$

Introduce $x' = x - d/2$, so that

$$\begin{aligned} N^{BB}(d) &= \exp\left(-\frac{d^2}{2(\sigma^{AB})^2}\right) \frac{(N^{AB})^2}{(\pi(\sigma^{AB})^2)^2} \iint_{xy} \exp\left(-\frac{2(x'^2 + y^2)}{(\sigma^{AB})^2}\right) dx dy \\ &= \exp\left(-\frac{d^2}{2(\sigma^{AB})^2}\right) \frac{(N^{AB})^2}{(\pi(\sigma^{AB})^2)^2} \sqrt{\frac{\pi(\sigma^{AB})^2}{2}} \sqrt{\frac{\pi(\sigma^{AB})^2}{2}} \\ &= \frac{(N^{AB})^2}{2\pi(\sigma^{AB})^2} \exp\left(-\frac{d^2}{2(\sigma^{AB})^2}\right), \end{aligned} \quad (51)$$

using the identity $\int_{-\infty}^{\infty} \exp(-ax^2) = \sqrt{\pi/a}$.

This result demonstrates that the number of shared connections between two neurons with Gaussian synaptic connection densities is itself a Gaussian function of the radial distance between the neurons with a variance that is half the value of the synaptic connection density radius. This means that a postsynaptic neuron is expected to have the most common connections with itself, for which $d = 0$. Additionally, for small variance or connection radius, a postsynaptic neuron will share many connections with proximate neighbors, with the number of shared connections falling off quickly with distance. Since the expected number of synaptic inputs is constant, a large connection radius implies that the neuron will have shared connections with neurons comparatively distal to it, since nearby neurons will have comparatively fewer shared connections.

Appendix B Variance of neural activity

To derive the variance in neural activity for a layer B neuron, it is necessary to consider that a single presynaptic neuron, say neuron m , in layer A may have multiple synaptic connections to a neuron i in layer B (see Fig. 1). Using the synaptic connection density in Eq. (1), we know that the expected number of synaptic connections between m and i , separated by a distance of $[x_{mi}, y_{mi}]$, is

$$N_{mi}^{AB} = \frac{N^{AB}}{\pi(\sigma^{AB})^2} \exp\left(-\frac{x_{mi}^2 + y_{mi}^2}{(\sigma^{AB})^2}\right). \quad (52)$$

From Eq. (6a), the expected variance of a neuron in layer B can be written as,

$$\begin{aligned} \text{var}(\langle f_i^B \rangle) &= \text{var}\left(\left\langle R_a^B + \sum_m w_{mi}^{BC} f_m^A \right\rangle\right) \\ &= N^{AB} \lambda^A + 2 \sum_m \sum_{n < m} \langle \text{cov}(f_m^A, f_n^A) \rangle, \end{aligned} \quad (53)$$

where we have assumed that weights between layers A and B have evolved to the upper bound of 1 (cf. Linsker (1986a)) and used the fact that $\text{var}\left(\sum_{i=1}^n a_i x_i\right) = \sum_{i=1}^n a_i^2 \text{var}(x_i) + 2 \sum_j \sum_{i < j} a_i a_j \text{cov}(x_i, x_j)$.

To determine the contribution of the covariance term in Eq. (53), we note that each pair of synapses originating from the same presynaptic neuron will be fully correlated, while synapses stemming from different presynaptic neurons in layer A will be uncorrelated. For neuron m in layer A with N_{mi}^{AB} synaptic connections to neuron i in layer B , there will be $\binom{N_{mi}^{AB}}{2} = N_{mi}^{AB} (N_{mi}^{AB} - 1) / 2 \approx (N_{mi}^{AB})^2 / 2$ synapse pairs contributing to the covariance sum. Consequently, the total contribution of neuron m to the covariance term in Eq. (53) will be $\frac{(N_{mi}^{AB})^2}{2} \lambda^A$. To obtain an expression for the variance of layer B neurons, we evaluate this expression using Eq. (52) and substitute it into Eq. (53). Applying a continuous spatial approximation to the layer, we can integrate to get the total expected contribution of all presynaptic neurons to the covariance term and evaluate Eq. (53),

$$\begin{aligned} \text{var}(\langle f_i^B \rangle) &= N^{AB} \lambda^A + \lambda^A \iint_{xy} N_{mi}^2 dx dy \\ &= N^{AB} \lambda^A + \lambda^A \iint_{xy} \left(\frac{N^{AB}}{\pi(\sigma^{AB})^2}\right)^2 \exp\left(-2\frac{x^2 + y^2}{(\sigma^{AB})^2}\right) dx dy \\ &= \lambda^A \left(N^{AB} + \frac{(N^{AB})^2}{2\pi(\sigma^{AB})^2}\right). \end{aligned} \quad (54)$$

Appendix C Covariance of neural activity

We wish to derive expressions for the covariance of layer B neurons. Sample covariance between two postsynaptic neuron rates in layer B , say f_i^B and f_j^B , for neurons i and j , respectively, is calculated as

$$\text{cov}(f_i^B, f_j^B) = \text{E}[f_i^B f_j^B] - \text{E}[f_i^B] \text{E}[f_j^B]. \quad (55)$$

For unitary weights from layer A to layer B , Eq. (6) can be employed to give

$$\begin{aligned}
\text{cov}(f_i^B, f_j^B) &= \mathbb{E}\left[\left(R_a^B + \sum_m f_m^A\right)\left(R_a^B + \sum_n f_n^A\right)\right] - \mathbb{E}\left[R_a^B + \sum_m f_m^A\right]\mathbb{E}\left[R_a^B + \sum_n f_n^A\right] \\
&= (R_a^B)^2 + 2R_a^B \overline{f^B} + \mathbb{E}\left[\sum_m \sum_n f_m^A f_n^A\right] - \left((R_a^B)^2 + 2R_a^B \overline{f^B} + (N^{AB} \overline{f^B})^2\right) \\
&= \left(\mathbb{E}\left[\sum_m \sum_n f_m^A f_n^A\right] - (N^{AB} \overline{f^B})^2\right).
\end{aligned} \tag{56}$$

Using the expression for the expected number of shared connections between layer B neurons in Eq. (3), the covariance is given by

$$\text{cov}(f_i^B, f_j^B) = \frac{(N^{AB})^2 (\lambda^A)^2}{2\pi(\sigma^{AB})^2} \exp\left(-\frac{d^2}{2(\sigma^{AB})^2}\right). \tag{57}$$

Appendix D Covariance of neural activity in the frequency domain

We express covariance between two stationary, real variates, x and y , as a function of their frequency domain counterparts, X and Y .

$$\gamma_{x,y}(\tau) = \frac{1}{T} \sum_t X(t) Y(t + \tau). \tag{58}$$

Similar to the convolution theorem, the cross-correlation theorem states that (Kumar, 2009)

$$\gamma_{x,y}(\tau) = \frac{1}{T^2} \sum_k (X(k))^* Y(k) \exp\left(2\pi i \tau \frac{k}{T}\right), \tag{59}$$

where $X(k)$ and $Y(k)$ denote the spectral variates of x and y , respectively, at frequency k .

Since instantaneous covariance is equivalent to the cross-correlation of zero-meaned variates at lag 0, we can express covariance between two layer B neurons as

$$\begin{aligned}
\text{cov}(f_i^B, f_j^B) &= \frac{1}{T^2} \sum_k (F_i^B(k))^* F_j^B(k) \exp\left(2\pi i 0 \frac{k}{T}\right) \\
&= \frac{1}{T^2} \sum_k (F_i^B(k))^* F_j^B(k).
\end{aligned} \tag{60}$$

Appendix E Derivation of delay in the frequency domain

We wish to calculate the expected value of delay in the frequency domain. This requires an expression of delay as a function of distance in the frequency domain and the probability of obtaining each distance. The product of these two functions can then be integrated over the laminar to give the expected value. Since we are finding the expected value in the frequency domain, we can expect values to be complex. Consequently, contour integration will be used.

To calculate the expected value of delay in the frequency domain, use $\mathbb{E}[d] = \int g(d)p(d)dr$ for some function, $g(d)$, of distance, d , with probability density, $p(d)$. Using the known distribution of distance, given in Eq. (4), the linear transformation from distance to delay, given in Eq. (5), and the expression of a temporal delay in the frequency domain, given by $\mathcal{F}\{x(t - \Delta)\} = X(k) \exp(-2\pi i \Delta k')$, the function can be identified as $g(d) = \exp\left(-2\pi i k'/T \frac{((d^{AB})^2 + d^2)^{1/2} \mu}{v}\right)$. Consequently, the expected value of delay in the frequency domain can be determined by evaluating

$$\mathbb{E}\left[\exp(-2\pi i \Delta k')\right] = \int_0^\infty \exp\left(-2\pi i k' \frac{((d^{AB})^2 + d^2)^{1/2} \mu}{v}\right) \frac{2d}{(\sigma^{AB})^2} \exp\left(-\frac{d^2}{(\sigma^{AB})^2}\right) dd, \tag{61}$$

where we have used $d_{mi}^B = d$. Introduce a change of variable, $r' = ((d^{AB})^2 + d^2)^{1/2}$, so that $dd = dr' (r'^2 - (d^{AB})^2)^{-1/2} r'$, and

$$\begin{aligned} \mathbb{E} \left[\exp(-2\pi i \Delta k') \right] &= \frac{2}{(\sigma^{AB})^2} \int_{d^{AB}}^{\infty} r' \exp\left(-2\pi i k' \frac{r' \mu}{v}\right) \exp\left(-\frac{r'^2 - (d^{AB})^2}{(\sigma^{AB})^2}\right) dr' \\ &= \frac{2}{(\sigma^{AB})^2} \exp\left(\frac{(d^{AB})^2}{(\sigma^{AB})^2}\right) \int_{d^{AB}}^{\infty} r' \exp\left(-\frac{r'^2}{(\sigma^{AB})^2}\right) \exp\left(-2\pi i k' \frac{r' \mu}{v}\right) dr'. \end{aligned} \quad (62)$$

$$(63)$$

This integral has the form $\int_{x_0}^{\infty} x e^{-ax^2} e^{-ibx} dx$, which we will use for the interim for readability. Using integration by parts,

$$\int_{x_0}^{\infty} f(x) g'(x) dx = f(x) g(x) \Big|_{x_0}^{\infty} - \int_{x_0}^{\infty} g(x) f'(x) dx, \quad (64)$$

and setting $g(x) = -\frac{1}{2a} e^{-ax^2}$, $f(x) = e^{-ibx}$, so that $g'(x) = x e^{-ax^2}$, and $f'(x) = -i b e^{-ibx}$, and

$$\begin{aligned} \int_{x_0}^{\infty} x e^{-ax^2} e^{-ibx} dx &= -\frac{1}{2a} e^{-ibx} e^{-ax^2} \Big|_{x_0}^{\infty} - \frac{1}{2a} \int_0^{\infty} i b e^{-ibx} e^{-ax^2} dx \\ &= +\frac{1}{2a} e^{-ax_0^2 - ibx_0} + \frac{ib}{2a} - \int_{x_0}^{\infty} e^{-(ax^2 + ibx)} dx. \end{aligned} \quad (65)$$

Since the integral in Eq. (65) is over a complex domain, it can be solved using contour integration. Cauchy's theorem states that, for an analytic function that is differentiable everywhere, a closed line integral of the function evaluates to zero. Consequently, in general,

$$0 = \oint e^{-ax^2} dx \quad (66)$$

$$= \int_{x_0}^{\infty} e^{-a(x+iz)^2} dx \Big|_{z=0} + i \int_0^p e^{-a(x+iz)^2} dz \Big|_{x=\infty} - \int_{x_0}^{\infty} e^{-a(x+iz)^2} dx \Big|_{z=p} - i \int_0^p e^{-a(x+iz)^2} dz \Big|_{x=0}, \quad (67)$$

$$(68)$$

where the contour is from $x_0 + i0 \rightarrow \infty + i0$, then $\infty + i0 \rightarrow \infty + ip$, from $\infty + ip \rightarrow x_0 + ip$, and finally $x_0 + ip \rightarrow x_0 + i0$. The second term on the right-hand side evaluates to 0 since it contains $e^{-\infty}$, so that

$$0 = \oint e^{-ax^2} dy \quad (69)$$

$$= \int_{x_0}^{\infty} e^{-ax^2} dy - \int_{x_0}^{\infty} e^{-a(x+ip)^2} dy - i \int_0^p e^{-a(x_0+iz)^2} dz. \quad (70)$$

$$(71)$$

Using the fact that $\int_{-\infty}^{\infty} e^{-ax^2} = \sqrt{\frac{\pi}{a}}$, in conjunction with e^{-ax^2} being a real function, we know that $\int_0^{\infty} e^{-ax^2} = \sqrt{\frac{\pi}{4a}}$. Therefore,

$$\begin{aligned} \int_{x_0}^{\infty} e^{-a(x+ip)^2} dx &= \int_{x_0}^{\infty} e^{-ax^2} dy - i \int_0^p e^{-a(x_0+iz)^2} dz \\ &= \sqrt{\frac{\pi}{4a}} \operatorname{erfc}(\sqrt{ax}) - i \sqrt{\frac{\pi}{4a}} (\operatorname{erf}(\sqrt{ap}(x_0 + ip)) - \operatorname{erf}(\sqrt{ax_0})) \\ &= \sqrt{\frac{\pi}{4a}} (\operatorname{erfc}(\sqrt{ax}) - i \operatorname{ierf}(\sqrt{a}(x_0 + ip)) + i \operatorname{ierf}(\sqrt{ax_0})) \end{aligned}$$

$$(72)$$

where we have used the definition of $\operatorname{erfi}(z) = \frac{2}{\sqrt{\pi}} \int_0^z e^{t^2} dt$, followed by $\operatorname{erfi}(z) = -\operatorname{ierf}(iz)$.

For the specific integral of $e^{-(ax^2+ibx)}$, set $p = \frac{b}{2a}$,

$$e^{-a(x+ip)^2} = e^{-a(x+i\frac{b}{2a})^2} \quad (73)$$

$$= e^{-ax^2-ibx} e^{\frac{b^2}{4a}}, \quad (74)$$

so that, from Eq. (72),

$$e^{-(ax^2+ibx)} e^{\frac{b^2}{4a}} = \sqrt{\frac{\pi}{4a}} \left(\operatorname{erfc}(\sqrt{ax}) - \operatorname{ierf}\left(\sqrt{a}\left(x+i\frac{b}{2a}\right)\right) + \operatorname{ierf}(\sqrt{ax_0}) \right), \quad (75)$$

or

$$e^{-ax^2} e^{-ibx} = e^{-\frac{b^2}{4a}} \sqrt{\frac{\pi}{4a}} \left(\operatorname{erfc}(\sqrt{ax}) - \operatorname{ierf}\left(\sqrt{ax_0+i\frac{b}{2\sqrt{a}}}\right) + \operatorname{ierf}(\sqrt{ax_0}) \right). \quad (76)$$

Substituting this result back into Eq. (65), we get

$$\begin{aligned} \int_{x_0}^{\infty} x e^{-ax^2} e^{-ibx} dx &= \frac{1}{2a} - \frac{ib\sqrt{\pi}}{4a^{3/2}} e^{-\frac{b^2}{4a}} \left(\operatorname{erfc}(\sqrt{ax_0}) - \operatorname{ierf}\left(\sqrt{ax_0+i\frac{b}{2\sqrt{a}}}\right) + \operatorname{ierf}(\sqrt{ax_0}) \right) \\ &= \frac{1}{2a} e^{-ax_0^2-ibx_0} - \frac{b\sqrt{\pi}}{4a^{3/2}} e^{-\frac{b^2}{4a}} \left(\operatorname{ierfc}(\sqrt{ax_0}) + \operatorname{erf}\left(\sqrt{ax_0+i\frac{b}{2\sqrt{a}}}\right) - \operatorname{erf}(\sqrt{ax_0}) \right). \end{aligned} \quad (77)$$

Applying this result to the original equation in Eq. (62) using $a = \frac{1}{(\sigma^{AB})^2}$, $b = 2\pi k' \frac{\mu}{v}$, and $x_0 = d^{AB}$, the expected value of delay between layers A and layer B is

$$\begin{aligned} D^{AB}(k) &= \mathbb{E} \left[\exp(-2\pi i \Delta k') \right] \\ &= \exp\left(-2\pi i k' \frac{d^{AB} \mu}{v}\right) \\ &\quad - \pi^{3/2} k' \frac{\sigma^{AB} \mu}{v} \exp\left(\frac{(d^{AB})^2}{(\sigma^{AB})^2}\right) \exp\left(-\left(\pi k' \frac{\sigma^{AB} \mu}{v}\right)^2\right) \left(\operatorname{ierfc}\left(\frac{d^{AB}}{\sigma^{AB}}\right) + \operatorname{erf}\left(\frac{d^{AB}}{\sigma^{AB}} + i\pi k' \frac{\sigma^{AB} \mu}{v}\right) - \operatorname{erf}\left(\frac{d^{AB}}{\sigma^{AB}}\right) \right). \end{aligned} \quad (78)$$

For $d^{AB} \gg \sigma^{AB}$, this reduces to $\mathbb{E} \left[\exp\left(-2\pi i k' \frac{d^{AB} \mu}{v}\right) \right]$ which has an absolute value of 1.

Appendix F Derivation of average covariance

F.1 Linsker's network

The average covariance between layer B neurons in the network assumed by Linsker (1986a) can be found by integrating the expression for covariance over the laminar,

$$\begin{aligned} \overline{Q^{BB}} &= \frac{1}{(\pi(\sigma^{BC})^2)^2} \int_{-\infty}^{\infty} \int_{-\infty}^{\infty} \exp\left(-\frac{|\mathbf{x}-\mathbf{x}'|^2}{2(\sigma^{AB})^2}\right) \exp\left(-\frac{(\mathbf{x}^2+\mathbf{x}'^2)}{(\sigma^{BC})^2}\right) d\mathbf{x}' d\mathbf{x} \\ &= \frac{1}{(\pi(\sigma^{BC})^2)^2} \exp\left(-\frac{\mathbf{x}^2}{\alpha}\right) \int_{-\infty}^{\infty} \int_{-\infty}^{\infty} \exp\left(-\frac{\mathbf{x}'^2}{\alpha}\right) \exp\left(\frac{\mathbf{x}'\mathbf{x}}{(\sigma^{AB})^2}\right) d\mathbf{x}' d\mathbf{x} \end{aligned} \quad (79)$$

where $\alpha = \frac{2(\sigma^{AB})^2(\sigma^{BC})^2}{2(\sigma^{AB})^2 + (\sigma^{BC})^2}$ for convenience. Furthermore, the radial symmetry of the covariance and probability connection functions renders the result directionally invariant. Therefore, we calculate the result in one dimension and square it to generalize it to two dimensions,

$$\begin{aligned}
\overline{Q^{BB}} &= \frac{1}{(\pi(\sigma^{BC})^2)^2} \left(\int_{-\infty}^{\infty} \exp\left(-\frac{x^2}{\alpha}\right) \exp\left(\frac{x^2\alpha}{4(\sigma^{AB})^4}\right) \int_{-\infty}^{\infty} \exp\left(-\left(\frac{x}{\alpha} - \frac{\sqrt{\alpha}\tilde{x}}{2(\sigma^{AB})^2}\right)^2\right) d\tilde{x} dx \right)^2 \\
&= \frac{\pi\alpha}{(\pi(\sigma^{BC})^2)^2} \left(\int_{-\infty}^{\infty} \exp\left(-\frac{x^2}{\alpha}\right) \exp\left(\frac{x^2\alpha}{4(\sigma^{AB})^4}\right) \exp(-\chi^2) d\chi dx \right)^2 \\
&= \frac{\alpha}{\pi(\sigma^{BC})^4} \left(\int_{-\infty}^{\infty} \exp\left(-x^2 \frac{4(\sigma^{AB})^4 - \alpha^2}{4(\sigma^{AB})^2\alpha}\right) dx \right)^2 \\
&= \frac{\alpha}{\pi(\sigma^{BC})^4} \left(\int_{-\infty}^{\infty} \exp\left(-x^2 \frac{2(\sigma^{AB})^2 + (\sigma^{BC})^2}{2(\sigma^{AB})^2(\sigma^{BC})^2 + (\sigma^{BC})^4}\right) dx \right)^2 \\
&= \frac{\alpha}{\pi(\sigma^{BC})^4} \left(\frac{\pi(2(\sigma^{AB})^2(\sigma^{BC})^2 + (\sigma^{BC})^4)}{2(\sigma^{AB})^2 + 2(\sigma^{BC})^4} \right)^2 \\
&= \frac{2(\sigma^{AB})^4 + (\sigma^{AB})^2(\sigma^{BC})^2}{2(\sigma^{AB})^4 + 3(\sigma^{AB})^2(\sigma^{BC})^2 + (\sigma^{BC})^4} \\
&= \frac{2 + \frac{(\sigma^{BC})^2}{(\sigma^{AB})^2}}{2 + 3\frac{(\sigma^{BC})^2}{(\sigma^{AB})^2} + \frac{(\sigma^{BC})^4}{(\sigma^{AB})^4}} \\
&= \frac{2 + \frac{(\sigma^{BC})^2}{(\sigma^{AB})^2}}{\left(2 + \frac{(\sigma^{BC})^2}{(\sigma^{AB})^2}\right) \left(1 + \frac{(\sigma^{BC})^2}{(\sigma^{AB})^2}\right)} \\
&= \frac{1}{1 + \frac{(\sigma^{BC})^2}{(\sigma^{AB})^2}}. \tag{80}
\end{aligned}$$

F.2 Network with propagation delay and arbitrary postsynaptic potential function

For a network that incorporates the impact of delay and an arbitrary PSP function, the average covariance of the pre-synaptic inputs to the post-synaptic neurons in layer C must be calculated using the expression for covariance between two filtered and delayed layer B neuron outputs, since the signals arrive at the synapse where learning is assumed to occur. This expression was determined in Eq. (33), where it was assumed that synapse weight changes are initiated near the cell body of the post-synaptic neuron. To calculate the average normalized covariance, Eq. (15), we use Cartesian coordinates, recognizing that the expression for covariance is circularly symmetric. Therefore, we determine the result for a single dimension and square it. We first find the average covariance for a neuron at position \mathbf{x} with all other neurons in the laminar, and then find the average across all neurons. Propagation delay for spikes between the pre-synaptic neuron at \mathbf{x} and the post-synaptic neuron in layer C can be expressed as $\Delta_{\mathbf{x}}^{BC} = \frac{((d^{BC})^2 + \|\mathbf{x}\|^2)^{1/2} \mu}{v}$, which can be approximated by $\Delta_{\mathbf{x}}^{BC} \approx \frac{\|\mathbf{x}\|^2}{2d^{BC}v}$ for inter-laminar distances, d^{BC} , significantly larger than the pre-synaptic neuron's radial distance to the post-synaptic neuron, $\|\mathbf{x}\|$. Mean covariance can then

be expressed as

$$\begin{aligned}
\overline{Q_{\Delta,\varepsilon}^{BB}} &\approx \frac{1}{\pi^2(\sigma^{BC})^4} \left(\int_{-\infty}^{\infty} dx \int_{-\infty}^{\infty} d\tilde{x} \exp\left(-\frac{x^2 + \tilde{x}^2}{2(\sigma^{AB})^2}\right) \exp\left(\frac{x\tilde{x}}{(\sigma^{AB})^2}\right) \exp\left(-\frac{x^2 + \tilde{x}^2}{(\sigma^{BC})^2}\right) \kappa_{\Delta x\tilde{x}}^{BC} \right)^2 \\
&= \frac{1}{\pi(\sigma^{BC})^4(\tau_\varepsilon^2 - \tau_D^2)^2} \left(\int_{-\infty}^{\infty} dx \int_{-\infty}^{\infty} d\tilde{x} \exp\left(-\frac{x^2 + \tilde{x}^2}{2(\sigma^{AB})^2}\right) \exp\left(\frac{x\tilde{x}}{(\sigma^{AB})^2}\right) \exp\left(-\frac{x^2 + \tilde{x}^2}{(\sigma^{BC})^2}\right) \right. \\
&\quad \times \left. \left(\exp\left(-\frac{|x^2 - \tilde{x}^2|}{2d^{BC}v\tau_\varepsilon}\right) \tau_\varepsilon - \exp\left(-\frac{|x^2 - \tilde{x}^2|}{2d^{BC}v\tau_D}\right) \tau_D \right) \right)^2 \\
&= \frac{1}{\pi(\sigma^{BC})^4(\tau_\varepsilon^2 - \tau_D^2)^2} \left[\int_{-\infty}^{\infty} dx \int_{-\infty}^x d\tilde{x} \exp\left(-\frac{x^2 + \tilde{x}^2}{2(\sigma^{AB})^2}\right) \exp\left(\frac{x\tilde{x}}{(\sigma^{AB})^2}\right) \exp\left(-\frac{x^2 + \tilde{x}^2}{(\sigma^{BC})^2}\right) \right. \\
&\quad \times \left. \left(\exp\left(-\frac{x^2 - \tilde{x}^2}{2d^{BC}v\tau_\varepsilon}\right) \tau_\varepsilon - \exp\left(-\frac{x^2 - \tilde{x}^2}{2d^{BC}v\tau_D}\right) \tau_D \right) \right. \\
&\quad + \left. \int_{-\infty}^{\infty} dx \int_x^{\infty} d\tilde{x} \exp\left(-\frac{x^2 + \tilde{x}^2}{2(\sigma^{AB})^2}\right) \exp\left(\frac{x\tilde{x}}{(\sigma^{AB})^2}\right) \exp\left(-\frac{x^2 + \tilde{x}^2}{(\sigma^{BC})^2}\right) \right. \\
&\quad \times \left. \left(\exp\left(-\frac{\tilde{x}^2 - x^2}{2d^{BC}v\tau_\varepsilon}\right) \tau_\varepsilon - \exp\left(-\frac{\tilde{x}^2 - x^2}{2d^{BC}v\tau_D}\right) \tau_D \right) \right]^2 \\
&= \frac{1}{\pi(\sigma^{BC})^4(\tau_\varepsilon^2 - \tau_D^2)^2} \left[\left(\int_{-\infty}^{\infty} dx \exp\left(-\frac{x^2}{\beta_\varepsilon^2}\right) \int_{-\infty}^x dx \exp\left(-\frac{\tilde{x}^2}{\tilde{\beta}_\varepsilon^2}\right) \exp\left(\frac{x\tilde{x}}{(\sigma^{AB})^2}\right) \tau_\varepsilon \right. \right. \\
&\quad - \left. \int_{-\infty}^{\infty} dx \exp\left(-\frac{x^2}{\beta_D^2}\right) \int_{-\infty}^x dx \exp\left(-\frac{\tilde{x}^2}{\tilde{\beta}_D^2}\right) \exp\left(\frac{x\tilde{x}}{(\sigma^{AB})^2}\right) \tau_D \right) \\
&\quad + \left(\int_{-\infty}^{\infty} dx \exp\left(-\frac{x^2}{\tilde{\beta}_\varepsilon^2}\right) \int_x^{\infty} dx \exp\left(-\frac{\tilde{x}^2}{\beta_\varepsilon^2}\right) \exp\left(\frac{x\tilde{x}}{(\sigma^{AB})^2}\right) \tau_\varepsilon \right. \\
&\quad \left. \left. - \int_{-\infty}^{\infty} dx \exp\left(-\frac{x^2}{\tilde{\beta}_D^2}\right) \int_x^{\infty} dx \exp\left(-\frac{\tilde{x}^2}{\beta_D^2}\right) \exp\left(\frac{x\tilde{x}}{(\sigma^{AB})^2}\right) \tau_D \right) \right]^2
\end{aligned} \tag{81}$$

where $\beta_\varepsilon^2 = \frac{2vd^{BC}\tau_\varepsilon(\sigma^{AB})^2(\sigma^{BC})^2}{vd^{BC}\tau_\varepsilon(\sigma^{BC})^2 + 2vd^{BC}\tau_\varepsilon(\sigma^{AB})^2 + (\sigma^{AB})^2(\sigma^{BC})^2}$, $\tilde{\beta}_\varepsilon^2 = \frac{2vd^{BC}\tau_\varepsilon(\sigma^{AB})^2(\sigma^{BC})^2}{vd^{BC}\tau_\varepsilon(\sigma^{BC})^2 + 2vd^{BC}\tau_\varepsilon(\sigma^{AB})^2 - (\sigma^{AB})^2(\sigma^{BC})^2}$, $\beta_D^2 = \frac{2vd^{BC}\tau_D(\sigma^{AB})^2(\sigma^{BC})^2}{vd^{BC}\tau_D(\sigma^{BC})^2 + 2vd^{BC}\tau_D(\sigma^{AB})^2 + (\sigma^{AB})^2(\sigma^{BC})^2}$, and $\tilde{\beta}_D^2 = \frac{2vd^{BC}\tau_D(\sigma^{AB})^2(\sigma^{BC})^2}{vd^{BC}\tau_D(\sigma^{BC})^2 + 2vd^{BC}\tau_D(\sigma^{AB})^2 - (\sigma^{AB})^2(\sigma^{BC})^2}$, all have units of m^2 and capture the extent of the radial spread of covariance between the layer B neurons with the PSP time constant, τ_ε and the propagation delay time constant, τ_D . The β^2 terms capture covariance of each x neuron in the layer with \tilde{x} neurons that are radially closer to the postsynaptic neuron (which, without loss of generality is assumed to be located at $(0,0)$). Conversely, the $\tilde{\beta}^2$ terms capture covariance of each x neuron with other neurons in the layer that are radially further from the postsynaptic

neuron. Complete the square in the exponent for \tilde{x} to obtain

$$\begin{aligned}
\overline{Q_{\Delta,\varepsilon}^{BB}}(x,y) &= \frac{1}{\pi(\sigma^{BC})^4(\tau_\varepsilon^2 - \tau_D^2)^2} \left[\int_{-\infty}^{\infty} dx \exp\left(-x^2 \left(\frac{1}{\beta_\varepsilon^2} - \frac{\tilde{\beta}_\varepsilon^2}{4(\sigma^{AB})^4}\right)\right) \int_{-\infty}^{x\left(\frac{1}{\beta_\varepsilon} - \frac{\tilde{\beta}_\varepsilon}{2(\sigma^{AB})^2}\right)} d\chi \beta_\varepsilon \exp(-\chi^2) \tau_\varepsilon \right. \\
&\quad - \int_{-\infty}^{\infty} dx \exp\left(-x^2 \left(\frac{1}{\beta_D^2} - \frac{\tilde{\beta}_D^2}{4(\sigma^{AB})^4}\right)\right) \int_{-\infty}^{x\left(\frac{1}{\beta_D} - \frac{\tilde{\beta}_D}{2(\sigma^{AB})^2}\right)} d\chi \beta_D \exp(-\chi^2) \tau_D \\
&\quad + \int_{-\infty}^{\infty} dx \exp\left(-x^2 \left(\frac{1}{\tilde{\beta}_\varepsilon^2} - \frac{\beta_\varepsilon^2}{4(\sigma^{AB})^4}\right)\right) \int_{x\left(\frac{1}{\tilde{\beta}_\varepsilon} - \frac{\beta_\varepsilon}{2(\sigma^{AB})^2}\right)}^{\infty} d\tilde{\chi} \tilde{\beta}_\varepsilon \exp(-\tilde{\chi}^2) \tau_\varepsilon \\
&\quad \left. - \int_{-\infty}^{\infty} dx \exp\left(-x^2 \left(\frac{1}{\tilde{\beta}_D^2} - \frac{\beta_D^2}{4(\sigma^{AB})^4}\right)\right) \int_{x\left(\frac{1}{\tilde{\beta}_D} - \frac{\beta_D}{2(\sigma^{AB})^2}\right)}^{\infty} d\tilde{\chi} \tilde{\beta}_D \exp(-\tilde{\chi}^2) \tau_D \right]^2 \\
&= \frac{1}{\pi(\sigma^{BC})^4(\tau_\varepsilon^2 - \tau_D^2)^2} \left[\int_{-\infty}^{\infty} dx \tau_\varepsilon \exp\left(-x^2 \left(\frac{1}{\beta_\varepsilon^2} - \frac{\tilde{\beta}_\varepsilon^2}{4(\sigma^{AB})^4}\right)\right) \left(1 + \operatorname{erf}\left(x \left(\frac{1}{\tilde{\beta}_\varepsilon} - \frac{\tilde{\beta}_\varepsilon}{(\sigma^{AB})^2}\right)\right)\right) \right. \\
&\quad - \int_{-\infty}^{\infty} dx \tau_D \exp\left(-x^2 \left(\frac{1}{\beta_D^2} - \frac{\tilde{\beta}_D^2}{4(\sigma^{AB})^4}\right)\right) \left(1 + \operatorname{erf}\left(x \left(\frac{1}{\tilde{\beta}_D} - \frac{\tilde{\beta}_D}{2(\sigma^{AB})^2}\right)\right)\right) \beta_D \\
&\quad + \int_{-\infty}^{\infty} dx \tau_\varepsilon \exp\left(-x^2 \left(\frac{1}{\tilde{\beta}_\varepsilon^2} - \frac{\beta_\varepsilon^2}{4(\sigma^{AB})^4}\right)\right) \operatorname{erfc}\left(x \left(\frac{1}{\tilde{\beta}_\varepsilon} - \frac{\beta_\varepsilon}{2(\sigma^{AB})^2}\right)\right) \tilde{\beta}_\varepsilon \\
&\quad \left. - \int_{-\infty}^{\infty} dx \tau_D \exp\left(-x^2 \left(\frac{1}{\tilde{\beta}_D^2} - \frac{\beta_D^2}{4(\sigma^{AB})^4}\right)\right) \operatorname{erfc}\left(x \left(\frac{1}{\tilde{\beta}_D} - \frac{\beta_D}{2(\sigma^{AB})^2}\right)\right) \tilde{\beta}_D \right]^2 \\
&= \frac{1}{\pi(\sigma^{BC})^4(\tau_\varepsilon^2 - \tau_D^2)^2} \left[\int_{-\infty}^{\infty} dx \tau_\varepsilon \exp\left(-x^2 \left(\frac{1}{\beta_\varepsilon^2} - \frac{\tilde{\beta}_\varepsilon^2}{4(\sigma^{AB})^4}\right)\right) \left(1 + \operatorname{erf}\left(x \left(\frac{1}{\tilde{\beta}_\varepsilon} - \frac{\tilde{\beta}_\varepsilon}{2(\sigma^{AB})^2}\right)\right)\right) \right. \\
&\quad - \int_{-\infty}^{\infty} dx \tau_D \exp\left(-x^2 \left(\frac{1}{\beta_D^2} - \frac{\tilde{\beta}_D^2}{4(\sigma^{AB})^4}\right)\right) \left(1 + \operatorname{erf}\left(x \left(\frac{1}{\tilde{\beta}_D} - \frac{\tilde{\beta}_D}{2(\sigma^{AB})^2}\right)\right)\right) \beta_D \\
&\quad + \int_{-\infty}^{\infty} dx \tau_\varepsilon \exp\left(-x^2 \left(\frac{1}{\tilde{\beta}_\varepsilon^2} - \frac{\beta_\varepsilon^2}{4(\sigma^{AB})^4}\right)\right) \left(1 - \operatorname{erf}\left(x \left(\frac{1}{\tilde{\beta}_\varepsilon} - \frac{\beta_\varepsilon}{2(\sigma^{AB})^2}\right)\right)\right) \tilde{\beta}_\varepsilon \\
&\quad \left. - \int_{-\infty}^{\infty} dx \tau_D \exp\left(-x^2 \left(\frac{1}{\tilde{\beta}_D^2} - \frac{\beta_D^2}{4(\sigma^{AB})^4}\right)\right) \left(1 - \operatorname{erf}\left(x \left(\frac{1}{\tilde{\beta}_D} - \frac{\beta_D}{2(\sigma^{AB})^2}\right)\right)\right) \tilde{\beta}_D \right]^2 \tag{82}
\end{aligned}$$

The error function components can be shown to integrate to 0, since $\int_{-\infty}^{\infty} \exp(-ay^2) \operatorname{erf}(ay) dy = 0$, giving

$$\begin{aligned}
\overline{Q_{\Delta,\varepsilon}^{BB}}(x,y) &= \frac{1}{(\sigma^{BC})^4(\tau_\varepsilon^2 - \tau_D^2)^2} \left[\tau_\varepsilon \beta_\varepsilon \left(\frac{1}{\beta_\varepsilon^2} - \frac{\tilde{\beta}_\varepsilon^2}{4(\sigma^{AB})^4}\right)^{-\frac{1}{2}} - \tau_D \beta_D \left(\frac{1}{\beta_D^2} - \frac{\tilde{\beta}_D^2}{4(\sigma^{AB})^4}\right)^{-\frac{1}{2}} \right. \\
&\quad \left. + \tau_\varepsilon \tilde{\beta}_\varepsilon \left(\frac{1}{\tilde{\beta}_\varepsilon^2} - \frac{\beta_\varepsilon^2}{4(\sigma^{AB})^4}\right)^{-\frac{1}{2}} - \tau_D \tilde{\beta}_D \left(\frac{1}{\tilde{\beta}_D^2} - \frac{\beta_D^2}{4(\sigma^{AB})^4}\right)^{-\frac{1}{2}} \right]^2 \\
&= \frac{1}{(\sigma^{BC})^4(\tau_\varepsilon^2 - \tau_D^2)^2} \left(\frac{\tau_\varepsilon (\beta_\varepsilon^2 + \tilde{\beta}_\varepsilon^2)}{\left(1 - \frac{\beta_\varepsilon^2 \tilde{\beta}_\varepsilon^2}{4(\sigma^{AB})^4}\right)^{\frac{1}{2}}} - \frac{\tau_D (\beta_D^2 + \tilde{\beta}_D^2)}{\left(1 - \frac{\beta_D^2 \tilde{\beta}_D^2}{4(\sigma^{AB})^4}\right)^{\frac{1}{2}}} \right)^2 \\
&= \frac{1}{(\sigma^{BC})^4(\tau_\varepsilon^2 - \tau_D^2)^2} \frac{\tau_\varepsilon^2 (\beta_\varepsilon^2 + \tilde{\beta}_\varepsilon^2)^2}{\left(1 - \frac{\beta_\varepsilon^2 \tilde{\beta}_\varepsilon^2}{4(\sigma^{AB})^4}\right)} + \frac{\tau_D^2 (\beta_D^2 + \tilde{\beta}_D^2)^2}{\left(1 - \frac{\beta_D^2 \tilde{\beta}_D^2}{4(\sigma^{AB})^4}\right)} - \frac{2\tau_D \tau_\varepsilon (\beta_\varepsilon^2 + \tilde{\beta}_\varepsilon^2) (\beta_D^2 + \tilde{\beta}_D^2)}{\left(1 - \frac{\beta_\varepsilon^2 \tilde{\beta}_\varepsilon^2}{4(\sigma^{AB})^4}\right)^{\frac{1}{2}} \left(1 - \frac{\beta_D^2 \tilde{\beta}_D^2}{4(\sigma^{AB})^4}\right)^{\frac{1}{2}}} \tag{83}
\end{aligned}$$

Substituting back in the definitions for β_{τ_ϵ} and $\tilde{\beta}_{\tau_\epsilon}$, β_D , and $\tilde{\beta}_D$ and simplifying gives

$$\overline{Q_{\Delta,\epsilon}^{BB}} = \frac{1}{(\tau_\epsilon - \tau_D)^2 (\tau_\epsilon + \tau_D)^2} \left(\frac{4 \left(2 + \frac{(\sigma^{BC})^2}{(\sigma^{AB})^2} \right) \tau_\epsilon^2}{\left(\frac{(\sigma^{BC})^2}{v d^{BC} \tau_\epsilon} - 2 \right) \left(\frac{(\sigma^{BC})^2}{v d^{BC} \tau_\epsilon} - 2 - 2 \frac{(\sigma^{BC})^2}{(\sigma^{AB})^2} \right) \left(\frac{(\sigma^{BC})^2}{v d^{BC} \tau_\epsilon} + 2 + \frac{(\sigma^{BC})^2}{(\sigma^{AB})^2} \right)} + \frac{4 \left(2 + \frac{(\sigma^{BC})^2}{(\sigma^{AB})^2} \right) \tau_D^2}{\left(\frac{(\sigma^{BC})^2}{v d^{BC} \tau_D} - 2 \right) \left(\frac{(\sigma^{BC})^2}{v d^{BC} \tau_D} - 2 - 2 \frac{(\sigma^{BC})^2}{(\sigma^{AB})^2} \right) \left(\frac{(\sigma^{BC})^2}{v d^{BC} \tau_D} + 2 + \frac{(\sigma^{BC})^2}{(\sigma^{AB})^2} \right)} \right). \quad (84)$$

The final expression for mean covariance between pre-synaptic inputs on arrival at the post-synaptic neuron is a function of the following components: the size of the radial propagation delay to inter-laminar propagation delay between layers A and B , captured in τ_D , the time constant of the exponential PSP, τ_ϵ , the ratio of the connectivity radii between each layer, $\frac{(\sigma^{BC})^2}{(\sigma^{AB})^2}$, the ratio of the connectivity radius between layers B and C to the inter-laminar propagation delay, $v d^{BC} \tau_D$, which captures the impact of propagation delay between layers B and C , and the ratio of the connectivity radius between layers B and C to the PSP, $v d^{BC} \tau_\epsilon$, which captures the temporal spread of incoming spike to layer C resulting from the PSP, relative to the propagation delay between layers B and C .

References

- M. M. Asl, A. Valizadeh, and P. A Tass. Dendritic and axonal propagation delays determine emergent structures of neuronal networks with plastic synapses. *Scientific Reports*, 7, 2017. URL <http://dx.doi.org/10.1038/srep39682>.
- A. N. Burkitt, H. Meffin, and D. B. Grayden. Study of neuronal gain in a conductance-based leaky integrate-and-fire neuron model with balanced excitatory and inhibitory synaptic input. *Biological Cybernetics*, 89:119–125, 2003.
- C. E. Carr and M. Konishi. Axonal delay lines for time measurement in the owl’s brainstem. *Proceedings of the National Academy of Sciences, USA*, 85:8311–8315, 1988.
- C. E. Davey, D. B. Grayden, G. F. Egan, and L. A. Johnston. Filtering induces correlation in fMRI resting state data. *NeuroImage*, 64:728–740, 2013.
- A. Eguchi, S. A. Neymotic, and S. M. Stringer. Color opponent receptive fields set-organize in a biophysical model of visual cortex via spike-timing dependent plasticity. *Frontiers in Neural Circuits*, 8(16), 2014.
- R. Kempter, W. Gerstner, and J. L. van Hemmen. Hebbian learning and spiking neurons. *Physical Review E*, 59(4):4498–4514, 1999.
- J. Kremkow, L. U Perrinet, C. Monier, JM. Alonso, A. Aertsen, Y. Frégnac, and G. S. Masson. Push-pull receptive field organization and synaptic depression: Mechanisms for reliably encoding naturalistic stimuli in V1. *Frontiers in Neural Circuits*, 11:10–37, 2016.
- R. Kumar. *Signals and systems*. PHI Learning Pvt. Ltd., 2009.
- C. Leibold and C. L. van Hemmen. Temporal receptive fields, spikes, and Hebbian delay selection. *Neural Networks*, 14: 805–813, 2001.
- C. Leibold, R. Kempter, and C. L. van Hemmen. How spiking neurons give rise to a temporal-feature map: From synaptic plasticity to axonal selection. *Physical Review E*, 65:1–20, 2001.
- R. Linsker. From basic network principles to neural architecture: Emergence of spatial-opponent cells. *Proceedings of the National Academy of Sciences, USA*, 83:7508–7512, 1986a.
- R. Linsker. From basic network principles to neural architecture: Emergence of orientation-selective cells. *Proceedings of the National Academy of Sciences, USA*, 83:8390–8394, 1986b.
- R. Linsker. From basic network principles to neural architecture: Emergence of orientation columns. *Proceedings of the National Academy of Sciences, USA*, 83:8779–8783, 1986c.

- D. J. MacKay and K. D. Miller. Analysis of Linsker's application of Hebbian rules to linear networks. *Network: Computation in Neural Systems*, 1:257–297, 1990.
- K. D. Miller. *Correlation-based models of neural development*, chapter 7, pages 267–352. Hillsdale, 1990.
- R. J. Pumphrey and J. Z. Young. The rates of conduction of nerve fibres of various diameters in cephalopods. *Journal of Experimental Biology*, 15:453–466, 1938.
- M. Saam and R. Eckhorn. Lateral spike conduction velocity in the visual cortex affects spatial range of synchronisation and receptive field size without visual experience: a learning model with spiking neurons. *Biological Cybernetics*, 83:L1–L9, 2000.
- D. Shoham, M. Hubener, S. Schulze, A. Grinvald, and T. Bonhoeffer. Spatio-temporal frequency domains and their relation to cytochrome oxidase staining in cat visual cortex. *Nature*, 385:529–533, 1997.
- R. Sinha, M. Hoon, J. Baudin, H. Okawa, R. Wong, and F. Rieke. Cellular and circuit mechanisms shaping the perceptual properties of the primate fovea. *Cell*, 168(3):413–426, 2017.
- P. Sun, K. Ueno, R. A. Waggoner, J. L. Gardner, K. Tanaka, and K. Cheng. A temporal frequency-dependent functional architecture in human v1 revealed by high-resolution fMRI. *Nature Neuroscience*, 10(11):1404–1406, 2007.
- L. Thibos, D. Still, and A. Bradley. Characterization of spatial aliasing and contrast sensitivity in peripheral vision. *Vision Research*, 36:249–258, 1996.
- A. Venkataraman, P. Lewis, P. Unsbo, and L. Lunstrom. Peripheral resolution and contrast sensitivity: Effects of stimulus drift. *Vision Research*, 133:145–149, 2017.
- V. Virsu, J. Rovamo, P. Laurinen, and R. Nasanen. Temporal contrast sensitivity and cortical magnification. *Vision Research*, 22:1211–1217, 1982.
- S. Wimbauer, O. G. Wensch, K. D. Miller, and J. L. van Hemmen. Development of spatiotemporal receptive fields of simple cells: II. Simulation and analysis. *Biological Cybernetics*, 77:463–477, 1997.
- S. Wimbauer, W. Gerstner, and J. L. van Hemmen. Analysis of a correlation-based model for the development of orientation-selective receptive fields in the visual cortex. *Network: Computation in Neural Systems*, 9:449–466, 1998.
- C. Zhao, R. Hata, J. Okamura, and G. Wang. Differences in spatial and temporal frequency interactions between central and peripheral parts of the feline area 18. *Cognitive Neuroscience*, 44(8):2635–2645, 2016.